UC Irvine
UC Irvine Previously Published Works

Title

Gestational Benzo[a]pyrene Exposure Destroys F1 Ovarian Germ Cells Through Mitochondrial Apoptosis Pathway and Diminishes Surviving Oocyte Quality

Permalink

Journal

ISSN

Authors

Malott, Kelli F
Leon Parada, Kathleen
Lee, Melody
et al.

Publication Date

DOI

Peer reviewed

Gestational Benzo[a]pyrene Exposure Destroys F1 Ovarian Germ Cells Through Mitochondrial Apoptosis Pathway and Diminishes Surviving Oocyte Quality

Kelli F. Malott,[*,†] Kathleen Leon Parada,[‡] Melody Lee,[§] Edward Swanson,[§] and Ulrike Luderer [ID][*,†,‡,§,1]

[*]Environmental Health Sciences Graduate Program, University of California, Irvine, Irvine, California 92617, USA; [†]Department of Environmental and Occupational Health, University of California, Irvine, Irvine, California 92617, USA; [‡]Department of Developmental and Cell Biology, University of California, Irvine, Irvine, California 92617, USA; and [§]Department of Medicine, University of California, Irvine, Irvine, California 92617, USA

[1]To whom correspondence should be addressed at Center for Occupational and Environmental Health, 100 Theory Drive, Suite 100, Irvine, CA 92617, USA. E-mail: uluderer@uci.edu.

ABSTRACT

Polycyclic aromatic hydrocarbons, including benzo[a]pyrene (BaP), are products of incomplete combustion. In female mouse embryos primordial germ cells proliferate before and after arriving at the gonadal ridge around embryonic (E) 10 and begin entering meiosis at E13.5. Now oocytes, they arrest in the first meiotic prophase beginning at E17.5. We previously reported dose-dependent depletion of ovarian follicles in female mice exposed to 2 or 10 mg/kg-day BaP E6.5–15.5. We hypothesized that embryonic ovaries are more sensitive to gestational BaP exposure during the mitotic developmental window, and that this exposure results in persistent oxidative stress in ovaries and oocytes of exposed F1 female offspring. We orally dosed timed-pregnant female mice with 0 or 2 mg/kg-day BaP in oil from E6.5–11.5 (mitotic window) or E12.5–17.5 (meiotic window). Cultured E13.5 ovaries were utilized to investigate the mechanism of BaP-induced germ cell death. We observed statistically significant follicle depletion and increased ovarian lipid peroxidation in F1 pubertal ovaries following BaP exposure during either prenatal window. Culture of E13.5 ovaries with BaP induced germ cell DNA damage and release of cytochrome c from the mitochondria in oocytes, confirming that BaP exposure induced apoptosis via the mitochondrial pathway. Mitochondrial membrane potential, oocyte lipid droplet (LD) volume, and mitochondrial-LD colocalization were decreased and mitochondrial superoxide levels were increased in the MII oocytes of F1 females exposed gestationally to BaP. Results demonstrate similar sensitivity to germ cell depletion and persistent oxidative stress in F1 ovaries and oocytes following gestational BaP exposure during mitotic or meiotic windows.

Key words: oocyte; mitochondria; lipid droplets; polycyclic aromatic hydrocarbons; oxidative stress; benzo[a]pyrene.

Polycyclic aromatic hydrocarbons (PAHs), such as benzo[a]pyrene (BaP), are products of incomplete combustion of organic materials. BaP is a known ovotoxicant that depletes ovarian follicles in rodents at all ages when exposed (Gulyas and Mattison, 1979; Lim et al., 2013; Matikainen et al., 2002; Mattison, 1980; Mattison and Thorgeirsson, 1979). PAHs require metabolic activation to exert their negative effects, and in most cases, undergo oxidation to produce metabolites that interact with cellular macromolecules (Xue and Warshawsky, 2005). Metabolism of BaP occurs through several well-known pathways; oxidation

by cytochrome P450 enzymes (CYP450) to produce dihydrodiol epoxides, the formation of a BaP radical cation by CYP450 peroxidases, and dihydrodiol-dehydrogenase oxidation to eventually lead to the formation of o-quinones through an NADP+-dependent mechanism (Xue and Warshawsky, 2005). An ancillary pathway for BaP metabolism occurs via prostaglandin endoperoxide synthase 2 using BaP as a very weak reducing co-substrate, resulting in the formation of quinones (Eling et al., 1990). Of the above pathways for BaP metabolism, the pathways resulting in the formation of quinones are capable of reduction-oxidation (redox) cycling, in the presence of superoxide, producing reactive oxygen species (ROS) (Xue and Warshawsky, 2005). ROS are highly reactive compounds that can act as intracellular signaling molecules, but in high concentrations, can be detrimental to the cell through oxidation of DNA, proteins, and lipids, causing irreparable damage and eventually cell death (Penning et al., 1996). We recently demonstrated that the female mouse embryonic ovary expresses enzymes required to metabolize BaP and that female embryos have higher concentrations of BaP metabolites than male embryos (Lim et al., 2022). Others have shown that BaP metabolite concentrations in offspring plasma, cerebral cortex, and hippocampus declined to undetectable levels by PND30 after exposure of pregnant rats to BaP via inhalation from E11–21 (Wu et al., 2003) and declined to nearly undetectable levels in plasma and hearts of offspring by PND13 after oral dosing of pregnant rats with BaP from E14–17 (Jules et al., 2012).

Primordial germ cell (PGC) precursors are the embryonic precursors of oocytes, arising in the mouse proximal epiblast around E6.5 (de Sousa Lopes et al., 2007). These proliferate and differentiate to PGCs and migrate to the gonadal ridge, where they arrive starting at approximately E9.5. In the female embryo, the now oogonia continue to proliferate in the differentiating ovary, then enter meiosis to form oocytes beginning at approximately E13.5 (Wear et al., 2016). The oocytes progress through meiosis, arresting at the diplotene stage of the first meiotic prophase beginning at approximately E17.5. Germ cell development in the fetal ovary produces a finite oocyte pool, the primary determinant of female fertility and reproductive lifespan. The developing ovary is particularly sensitive to germ cell and follicle destruction by PAHs, and exposure to BaP during germ cell development diminishes the number of oocytes in the ovary (Lim et al., 2013, 2016; Lim and Luderer, 2018; Matikainen et al., 2002).

In mice, germ cell nest breakdown and follicular organization in the embryonic ovary begins shortly before birth (Pepling and Spradling, 2001; Wear et al., 2016). Oocytes are organized into follicles, surrounded by a few squamous granulosa cells, these primordial follicles constitute the ovarian reserve (Pepling, 2012; Pepling et al., 2007). Folliculogenesis supports the growth and maturation of a meiotically and developmentally competent oocyte. As the oocyte grows in volume throughout folliculogenesis, with the help of supportive granulosa cells, it is stockpiles maternal mRNAs, proteins, metabolites, antioxidants, and lipids in the form of lipid droplets (LDs) (Paczkowski et al., 2014; Valsangkar and Downs, 2013). Granulosa cells import lipids and metabolites from the follicular fluid. As the follicle grows, metabolites and lipids are exported from granulosa cells into the oocyte, and the oocyte is also capable of de novo lipogenesis (Aizawa et al., 2019; Prates et al., 2014; Zhang et al., 2020). Additionally, the oocyte expands its organelle population, particularly the mitochondria and LDs, both of which are crucial to the developmental competence of an oocyte (Bradley and Swann, 2019; Coticchio et al., 2004; Ramalho-Santos and Amaral, 2013). The fully mature, healthy ovulated mouse oocyte

contains roughly 100 000 mitochondria (Adhikari et al., 2022; Chiaratti et al., 2018).

Mitochondria are a primary source of ROS in the cell, converting 0.2%–2% of oxygen taken up by the cell into ROS (Ramalho-Santos et al., 2009). Electrons moving along the electron transport chain can react directly with oxygen, or other electron acceptors, creating free radicals. These free radicals can then be sequestered by antioxidants or react with macromolecules (lipids, DNA, proteins) in the cell causing damage. As outlined previously, the formation of BaP metabolites, such as quinones, can be particularly damaging as they are a class of redox cycling molecules, producing excess ROS, including superoxide, hydrogen peroxides, and hydroxyl radicals (Forman et al., 2009). LDs are monophospholipid organelles that contain a neutral lipid core consisting of triacylglycerol and cholesterol (Walther and Farese, 2009, 2012). The oxidation of lipids through fatty acid β-oxidation has been shown to be important to preimplantation development (Dunning et al., 2010); additionally they are believed to play several other important roles crucial to oocyte competence and preimplantation development, from supplying lipoic acid as a cofactor for metabolism (Jarc and Petan, 2019) to secondary signaling molecules (Prates et al., 2014).

The redox state of a cell refers to the relative concentrations of oxidized versus reduced intracellular components. Additionally, the balance between ROS and antioxidants has a significant role in determining this state (Devine et al., 2012). Oxidative stress occurs when the balance between ROS and antioxidant systems shifts in favor of ROS (Devine et al., 2012). When a cell is under oxidative stress for an extended period, BAX proteins oligomerize and insert into the mitochondrial membrane, creating a channel releasing cytochrome c, resulting in activation of the effector caspase-3, which drives intrinsic apoptosis (Orrenius et al., 2007). Mitochondrial apoptosis seems to be involved in postnatal decline in female germ cell populations (Matikainen et al., 2002). However, cells can exist for extended periods of time in a more oxidized state, without the induction of apoptosis (Devine et al., 2012). This persistent oxidative stress is still harmful to the cell, often resulting in oxidation of macromolecules such as proteins, DNA, and lipids (Devine et al., 2012). We can visualize the peroxidation of lipids in cells using the marker 4-hydroxynonenal (4-HNE), which is generated from the oxidation of lipids such as arachidonic and linoleic acids (Zhong and Yin, 2015).

Previously, we demonstrated that treatment of pregnant mice with BaP from E6.5–15.5 dose-dependently decreases fertility and results in fewer follicles in peripubertal and adult female offspring, with female Gclm null mice, deficient in GSH, being more sensitive to prenatal BaP exposure (Lim et al., 2013). These data suggest that fetal ovaries exposed in utero to BaP during PGC development were subject to BaP-induced PGC death. To understand the mechanism of BaP-induced germ cell death, we demonstrated that BaP exposure of cultured E13.5 ovaries concentration-dependently induced germ cell death through increased expression of BAX protein at 6 h and increased activation of caspases-9 and -3 at 24 h of exposure, without affecting PGC proliferation (Lim et al., 2016). We further demonstrated that BaP exposure resulted in concentration-dependent decreases in PGC number after 48 h exposure (Lim et al., 2016). Although these findings provide strong evidence of mitochondrial involvement in BaP-induced germ cell death, this pathway has yet to be fully characterized.

In this study, we hypothesize that F1 germ cells are more sensitive to BaP-induced depletion during proliferation

compared with meiosis, that BaP-induced depletion is mediated through increased oxidative stress leading to mitochondrial-driven apoptosis in the embryonic ovary, and that gestational BaP exposure reduces the development competence of oocytes by reducing their lipid stores, thus altering their oxidative state.

MATERIALS AND METHODS

Animals. Eight-week-old C57BL/6J females and males were purchased from Jackson Laboratories and acclimated for 2 weeks. Mice for these experiments were housed in an American Association for the Accreditation of Laboratory Animal Care-accredited facility at the University of California Irvine (UC Irvine), with free access to deionized water and soy-free laboratory chow (Harlan Teklad, 2919), on a 14:10 h light-dark cycle. Temperature was maintained at 21°C–23°C. The experimental protocols were carried out in accordance with the Guide for the Care and Use of Laboratory Animals and were approved by the Institutional Animal Care and Use Committee at UC Irvine (NRC, 2011).

BaP exposure. Females were singly housed and estrous cycles were assessed once a day at 10:00 AM by light microscopic examination of vaginal lavage fluid with 0.9% sodium chloride (Lim *et al.*, 2013). Females were caged with males on the afternoon of proestrus and the next morning pregnancy was confirmed by the presence of a vaginal plug and designated as embryonic day 0.5 (E0.5). Dams were treated by oral dosing via pipet inserted into the cheek pouch (Lim *et al.*,, 2022) with 0 or 2 mg/kg/day of BaP in sesame oil or oil vehicle alone from either E6.5–11.5 (Oil 6.5 and BaP 6.5) or E12.5–17.5 (Oil 1 2.5 and BaP 12.5), roughly corresponding to either entirely proliferative or mostly meiotic phases of germ cell development, respectively. F0 dams were allowed to give birth to the F1 generation (Figure 1A).

Embryonic ovary culture. Female C57BL/6J mice were mated, upon confirmation of proestrus, with a C57BL/6J male. The following morning was designated E0.5 upon confirmation of a vaginal plug. Pregnant dams were humanely euthanized on E13.5 using CO_2 overdose, and uteri were quickly removed. The ovaries, with attached mesonephros (hereafter referred to as ovaries), were removed from each female embryo (Figure 1B).

Each ovary was assigned to a treatment group, taking care that the individual ovaries from embryos of the same pregnant dam were distributed across exposure groups and no 2 ovaries from 1 embryo were allocated to the same exposure group. Ovaries were assigned to 4 concentration groups: uncultured, 0, 500, and 1000 ng/ml BaP dissolved in 0.005% DMSO (UC, DMSO, 500 ng/ml, and 1000 ng/ml, respectively). Ovaries were cultured on 0.4 μm Millicell-CM biopore membranes floating on culture medium at 37°C in 95% air and 5% CO_2 as described previously (Lim *et al.*, 2016; Lim and Luderer, 2018). E13.5 ovaries were cultured for 6 h then fixed in Bouin's fixative (Ricca chemical, 1120-16) for 90 min prior to storing in optimal cutting temperature (OCT) compound (Sakura, 4583) at −80°C.

Puberty onset and ovarian histomorphometry. F1 females were followed daily for vaginal opening, an indicator of the onset of puberty, beginning at weaning on PND 21, followed by daily vaginal cytology until the first day with cornified vaginal cytology typical of estrus, considered to be the best indicator of puberty in female mice (Safranski *et al.*, 1993). Vaginal lavage was performed with 0.9% sodium chloride. Lavage fluid was immediately examined using a light microscope, and predominant cell types were recorded (Cooper *et al.*, 1993). One female per F1 litter was sacrificed via CO_2 overdose and cervical dislocation on the morning of her first estrus. One ovary per female was fixed in Bouin's fixative overnight at 4°C. After fixation, ovaries were washed 3 times with 50% ethanol, then stored in 70% ethanol. Ovaries were embedded in glycol methacrylate resin (Technovit 8100, EMS, 14654) and sectioned at 20 μm for follicle counting. The second ovary was fixed overnight in 4% paraformaldehyde at 4°C then incubated in 30% sucrose at 4°C for at least 90 min and embedded in OCT compound.

Follicles were enumerated using StereoInvestigator software (MBF Biosciences) and an Olympus BX40 light microscope equipped with a motorized stage and 40× oil immersion objective. Small follicle counts were assessed by an investigator blind to experimental group using methods described previously (Luderer *et al.*, 2022; Myers *et al.*, 2004). Briefly, small (primordial and primary) follicles were counted in every 5th section from the start of the ovarian tissue, giving sampling fraction 1 (f1) = 1/5. For the second sampling fraction, the counting frame (measuring 175·175 μm) was superimposed over the section with a sampling grid (measuring 250·250 μm), giving (f2) = 30 625/62 500. For the final sampling fraction, 10 μm within the section, with an original thickness of 20 μm was the sample thickness counted; it is important to note that section thickness shrinks slightly with tissue staining, and the average section thickness across all sections measured came to 17.76 μm. The final sampling fraction is determined by the software after bringing the sample into focus: f(3) = 10/average section thickness. Total counts were multiplied by the reciprocals of the sampling fractions $Q^-_{(follicle)} \cdot (1/f1) \cdot (1/f2) \cdot (1/f3)$ to arrive at a total estimated number of follicles per ovary. Only follicles with a visible oocyte nucleus within the 10 μm sampling height were counted. Primordial follicles were characterized by the presence of a single layer of flattened granulosa cells with no more than 1 cuboidal granulosa cell. A follicle was primary if 2 or more granulosa cells were cuboidal, and the oocyte was surrounded by 4 or more granulosa cells in total. To assess large follicles, every section was counted using an Olympus BX60 brightfield microscope. A follicle was classified as secondary if the oocyte was surrounded by more than 1 layer of cuboidal granulosa cells, and an antral follicle was characterized by the presence of an antral cavity or several fluid-filled vesicles.

Immunohistochemistry. We previously validated antibodies for lipid peroxidation marker 4-hydroxynonenal (4-HNE) (Alpha Diagnostics, HNE11-S) and phosphorylated histone 2AX (ɣH2AX) (Cell Signaling Technologies, S139) (Lim and Luderer, 2018; Mishra *et al.*, 2016). Paraformaldehyde-fixed F1 pubertal ovaries and Bouin's-fixed E13.5 ovaries were embedded in OCT, sectioned at 10 μm, and stored at −80°C. Slides underwent antigen retrieval in 10 mM sodium citrate with 0.05% Tween-20 for 15 or 25 min, dependent on the antigen, at 95°C, followed by blocking with avidin and biotin (Vector Laboratories, SP-2001) and normal goat serum, then incubated with primary antibodies for 4-HNE (1:300, F1 ovaries only), ɣH2AX (1:500, E13.5 and F1 ovaries), or PUMA (1:200, E13.5 ovaries only) (Abcam, AB9643) raised in rabbit. Then slides were incubated with secondary anti-rabbit IgG, blocked with 0.3% H_2O_2, incubated with ABC reagent (Vector Laboratories, PK-4001), and immunostaining was visualized with diaminobenzidine substrate in peroxide buffer. Sections were counterstained with hematoxylin. The following controls were used for each experimental run (1) primary and secondary antibodies omitted, (2) primary antibody without
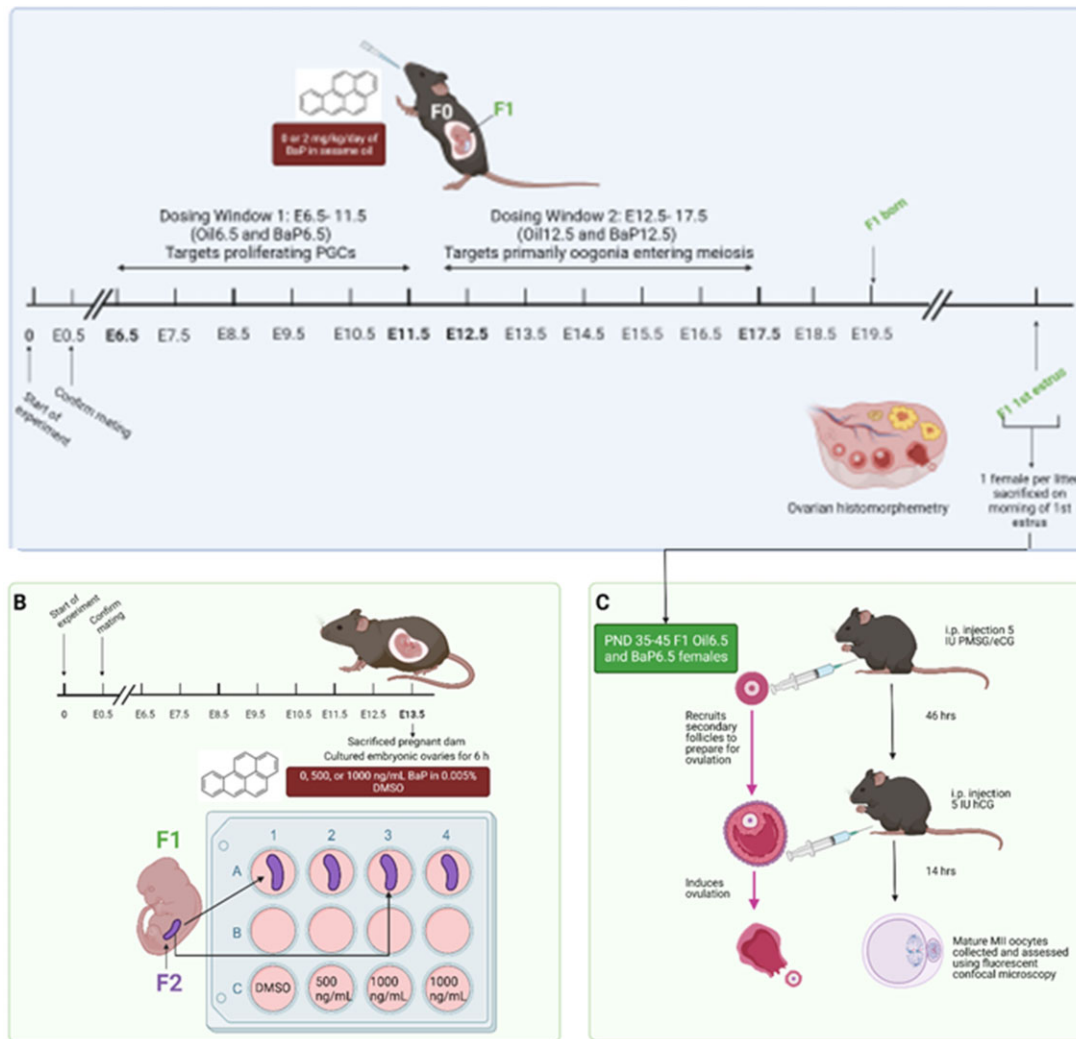
Experimental Design

Figure 1. A, Experimental design for *gestational* BaP exposure and assessment of F1 ovarian effects during 2 critical windows of ovarian development. B, Experimental design for *in vitro* BaP exposure and assessment of induction of mitochondrial apoptosis pathway. C, Experimental design for F1 *gestational* BaP exposure and assessment of F1-derived MII oocyte oxidative stress and developmental competence. All details of each exposure and endpoint are described in the Materials and Methods. Figure was created with the help of Biorender.com.

secondary antibody, (3) secondary antibody without primary antibody, and (4) nonimmune IgG in place of primary antibody.

Scoring for immunostaining was performed by an investigator blind to experimental group. Three independent experimental runs were performed with 1 slide per ovary, and 4 sections per slide were performed for each end point. 4-HNE staining was assessed using ImageJ FIJI (NIH). Images underwent a color-balance correction, then 4-HNE signal was measured over the total ovarian section and reported as reciprocal intensity per ovarian section area. For ɣH2AX staining in F1 pubertal ovaries, the percentages of primary, secondary, and antral follicles with positive granulosa cells or oocyte were counted per ovary section and averaged per ovary. For E13.5 ovaries, the percentages of positive ɣH2AX oocytes per ovary section were counted and assigned to meiosis stage, determined by the chromatin morphology (Láscarez-Lagunas *et al.*, 2020), then averaged per ovary. PUMA is ubiquitously expressed in the E13.5 ovary (Myers *et al.*, 2014). Therefore, total reciprocal intensity per ovarian section area was used to assess PUMA expression in E13.5 ovaries.

Immunofluorescence. Bouin's-fixed E13.5 ovaries were embedded in OCT and sectioned at 10 μm. Slides were incubated for 15 min in 10 mM sodium citrate with 0.05% Tween-20 for 15 min at 95°C for antigen retrieval, then incubated with avidin and biotin, and MOM blocking reagent (Vector Laboratories, FMK-2201). Ovaries were stained with mouse anti-cytochrome c (1:200) (Santa Cruz, SC-13156) and rabbit anti-germ cell nuclear antigen (GCNA) (1:200) (Abcam, AB82527) in MOM diluent (Vector Laboratories, FMK-2201) overnight at 4°C. The next day, slides were washed with 1× phosphate-buffered saline (PBS), incubated with anti-mouse Alexa Fluor 555 (Invitrogen, A21424) and anti-rabbit Alexa Fluor 647 (Invitrogen, A21247) for 1 h, and then coverslips were mounted with Prolong Gold (Invitrogen, P36934).

Ovary sections were imaged using an Elyra 7 with Lattice SIM (Carl Zeiss). Z-stack images were taken with 12 slices per image. Three images per ovarian section were taken at least 50 μm distance apart. Images were processed using standard fixed sample SIM^2 processing applied to each image. Images were analyzed for release of cytochrome c from the

mitochondria of oocytes using Imaris Imaging Software (Bitplane). Cytochrome c and GCNA fluorescence was used to generate 3-dimensional volumes. Cytochrome c volumes in close proximity to GCNA volumes (about $1\,\mu m$) were considered to be within the oocyte and were selected for analysis, whereas cytochrome c volumes further away from GCNA volumes were assumed to be somatic cells and were filtered out. Cytochrome c volumes proximal to GCNA surfaces were further filtered to distinguish between punctate versus diffuse staining, with diffuse staining determined to be indicative of release of cytochrome c into the germ cell cytosol (Feng et al., 2012; Liu et al., 2003). Diffuse cytochrome c volumes were defined as volumes greater than $1.73\,\mu m^3$ (Motta et al., 2000).

Superovulation. Postnatal day (PND) 35–45 F1 females exposed *in utero* to 0 or 2 mg/kg/day BaP from E6.5–11.5 were primed by i.p. injection with 5 IU equine chorionic gonadotropin (eCG) (Prospec Protein Specialists, Israel, HOR-272) at 1800 h; 46 h later superovulation was induced by an i.p. injection with 5 IU human chorionic gonadotropin (hCG) (Sigma Aldrich, CG10) (Figure 1C). Cumulus-oocyte complexes were harvested from the ampullae of the oviducts 14 h later following CO_2 euthanasia into flushing and holding medium (FHM) (Neta Scientific, MR-122-D). Oocytes were dissociated from the cumulus clouds by incubation in 0.3 mg/ml of hyaluronidase (ThermoFisher Scientific) for no more than 5 min, then immediately transferred to FHM under mineral oil (Sigma-Aldrich, M8410) for assessment. Only healthy, morphologically normal oocytes were chosen. Morphologically healthy oocytes were defined as having clear, granular cytoplasm; small perivitelline space; first polar body; colorless zona pellucida; not fragmented.

Oocyte staining and imaging. To measure the ratio of oxidized: unoxidized lipids, healthy oocytes were incubated in $10\,\mu M$ BODIPY 581/591 C11 (ThermoFisher, D3861) at 37°C and 5% CO_2 for 30 min under mineral oil, then subsequently washed through 3 droplets of FHM. Oocytes were imaged in glass-bottomed petri dishes in $50\,\mu l$ droplets of FHM without phenol red under mineral oil. BODIPY 581/591 C11 colocalizes with fatty acids inside the cell; upon oxidation of the polyunsaturated butadienyl portion, the fluorescence emission peak shifts from approximately 590 to approximately 510 nm, this red-to-green fluorescence shift allows for the use of green: red ratio reporting of oxidized lipids.

To measure the total neutral lipid content, mature oocytes were fixed with 4% paraformaldehyde for 1 h at room temperature, then washed through 3 droplets of $1\times$ PBS with 3 mg/ml of polyvinylpyrrolidone (PVP) (Sigma Aldrich, P0930). Fixed oocytes were incubated in $3.82\,\mu M$ of BODIPY 493/503 (4,4-difluoro-1, 3, 5, 7, 8-pentamethyl-4-bora-3a, 4a-diaz-s-indacene; ThermoFisher, D3922) for 1 h at room temperature under mineral oil, washed through 3 droplets of $1\times$ PBS with 3 mg/ml PVP, then imaged in glass-bottomed petri dishes in $50\,\mu l$ droplets of $1\times$ PBS under mineral oil. BODIPY 493/503 is a nonpolar lipid stain. Total LD content per oocyte was estimated by the sum fluorescence of LDs per cell. This was calculated by totaling the mean fluorescence intensity of LDs per cell estimated by Imaris Imaging Software (Bitplane). Average LD volume was estimated by creating 3D volumes using Imaris Imaging Software.

To assess mitochondrial membrane potential ($\Delta\Psi m$), we used the JC-1 (5,5′,6,6′-tetrachloro-1,1′,3,3′-tetraethyl-benzimidazolylcarbocyanine iodide) probe (ThermoFisher, T3168). Healthy oocytes were incubated in $5\,\mu M$ of JC-1 for 15 min at 37°C and 5% CO_2 under mineral oil, subsequently washed

through 3 consecutive droplets of FHM, prior to imaging on a glass-bottomed petri dish in $50\,\mu l$ droplet of FHM under mineral oil. Positive control oocytes were incubated in $1\,\mu M$ of CCCP (carbonyl cyanide 3-chlorophenylhydrazon; Millipore Sigma, C2759) under mineral oil for 15 min at 37°C, with atmosphere of 95% air, 5% CO_2. CCCP is a known mitochondrial uncoupler, which breaks down the $\Delta\Psi m$ by transporting protons across the inner mitochondrial membrane (Kasianowicz et al., 1984). JC-1 is a cationic carbocyanine dye that accumulates in the mitochondria. In low concentrations, the dye stays in its j-monomer form and will fluoresce green, however in high concentrations the dye will form j-aggregates that fluoresce red. Due to its cationic nature, the concentration of JC-1 per organelle is dependent on the $\Delta\Psi m$, thus, under lower $\Delta\Psi m$, it will fluoresce green and under high $\Delta\Psi m$, red. Total $\Delta\Psi m$ per oocyte is reported as the total sum fluorescence ratio of red: green.

MitoSOX (ThermoFisher, M36008) was used to assess mitochondrial superoxide production in live oocytes. Healthy oocytes were incubated in $5\,\mu M$ of MitoSOX for 30 min at 37°C and 5% CO_2 under mineral oil, then washed through 3 droplets of FHM prior to imaging on a glass-bottomed petri dish in $50\,\mu l$ droplet of FHM under mineral oil. MitoSOX is a fluorogenic dye specifically targeted to the mitochondria where it is immediately oxidized by superoxide specifically, if present, emitting red fluorescence. Mitochondrial superoxide production was estimated by total red fluorescence per oocyte. To measure oocyte GSH content, healthy oocytes were incubated in $1.5\,\mu M$ of monochlorobimane for 15 min at 37°C and 5% CO_2 under mineral oil, then washed through 3 droplets of FHM prior to imaging on a glass-bottomed petri dish in $50\,\mu l$ droplet of FHM under mineral oil. Oocyte GSH was estimated by total blue fluorescence per oocyte.

For colocalization of mitochondria and LDs, oocytes were incubated in 300 nM of MitoTracker Deep Red (ThermoFisher, M22426) at 37° C, with atmosphere of 95% air, 5% CO_2 for 30 min under mineral oil, then fixed in 4% paraformaldehyde at room temperature for 1 h, in darkness. Following fixation, oocytes were washed through 3 small droplets of $1\times$ PBS with 3 mg/ml PVP then incubated in $3.82\,\mu M$ BODIPY 493/503 under mineral oil for 1 h at room temperature in darkness. Following that incubation, oocytes were washed through 3 small droplets of $1\times$ PBS with 3 mg/mL PVP. Oocyte mitochondria were immediately imaged using confocal microscopy at 644/665 (ex/em) and oocyte LDs were visualized using 493/503 (ex/em).

Oocyte images were taken in z-stacks, using $63\times$ oil objective on a Zeiss 2-photon laser scanning microscope (LSM) 780 (ZEISS Research Microscopy Solutions), and all imaging analysis was performed using Imaris imaging software (Bitplane) or FIJI ImageJ (NIH). Analysis of $\Delta\Psi m$, mitochondria, and LDs were performed in Imaris Imaging Software by using the raw fluorescence to render volumes specific to the fluorescence wavelength. Unless otherwise specified, the mean fluorescence of each individual surface was calculated and the sum fluorescence for the whole oocyte was calculated. Mitosox fluorescence was analyzed in FIJI by compressing the z-stack, subtracting background fluorescence, then measuring the fluorescence in a region of interest encompassing the oocyte.

Statistical analyses. Data are displayed as means $\pm$ SEM unless otherwise noted. Effects of BaP exposure on ovarian histological endpoints were analyzed using 2-way ANOVA. Effects of prenatal BaP exposure on age at puberty onset were analyzed using generalized estimating equations (GEE), a form of general linear model, to account for litter effects, and estimated marginal

means and standard errors from the GEE models are reported. The effects of BaP exposure on oocyte endpoints were analyzed using GEE to account for repeated measures within animals (the same endpoint was measured in multiple oocytes from the same mouse). GEE models utilized exchangeable correlation matrices. In cases when the Hessian matrix did not converge for a GEE model, ANOVA with a random effect variable to account for multiple measurements within an animal was used. Endpoints expressed as percentages were analyzed using the nonparametric Kruskal Wallis test, and if statistically significant, was followed by Mann-Whitney tests for intergroup comparisons. IBM SPSS Statistics 25 for Macintosh was used for statistical analyses.

RESULTS

Germ Cell Death in Embryonic Ovaries Cultured With BaP Is Driven by Mitochondrial-Mediated Apoptosis

To further characterize the mechanism underlying BaP-induced germ cell death in fetal ovaries, we used an *in vitro* model in E13.5 ovaries. BaP metabolism results in the generation of various reactive metabolites, some of which directly react with DNA, forming bulky adducts and resultant DNA damage, whereas others redox cycle, generate ROS and cause oxidative DNA damage (Penning et al., 1996; Xue and Warshawsky, 2005). To detect DNA damage in exposed germ cells, we cultured E13.5 ovaries in 0, 500, and 1000 ng/ml of BaP in 0.005% DMSO for 6 h and tested whether BaP exposure led to increased DNA damage. Phosphorylation of histone H2AX (ɣH2AX) occurs rapidly adjacent to DNA double-strand breaks (Kinner et al., 2008). We observed that both concentrations of BaP (500 and 1000 ng/ml) resulted in statistically significant increases in the percentage of ɣH2AX-positive germ cells compared with DMSO and uncultured controls ($p = .002$, effect of experimental group by Kruskal-Wallis test, Figure 2A). Further, when positive germ cells were assessed for meiosis stage, to account for DNA DSBs that occur during meiosis, exposed ovaries had statistically significant increases in ɣH2AX-positive germ cells compared with DMSO and uncultured controls during interphase and leptotene, the meiotic stages when DSBs are normally not present ($p = .007$ and $p = .009$, respectively, by Kruskal-Wallis test, Figure 2B), demonstrating that BaP metabolism leads to increased DNA damage in embryonic ovaries.

p53-upregulated modulator of apoptosis (PUMA), a BH3 domain only BCL2 family pro-apoptosis regulator, is ubiquitously expressed in E13.5 ovaries (Myers et al., 2014). It is thought to regulate germ cell loss shortly after the conclusion of the migratory phase of germ cell development, but not during germ cell nest breakdown (Myers et al., 2014). DNA damage has been shown to trigger the mitochondrial apoptosis pathway through induction of PUMA. To further characterize this mechanism of cell death, we observed that *in vitro* BaP-exposure slightly, though not statistically significantly, increased PUMA expression in the whole embryonic ovary at 6 h (Figs. 3A and 3B).

Release of cytochrome c from the mitochondria to the cytosol, where it combines with apoptotic protease-activating factor 1 (APAF1) to form the apoptosome, is a key event of the mitochondrial apoptosis pathway (Ferraro et al., 2003). To confirm the activation of the mitochondrial apoptosis pathway, cytochrome c in germ cells was assessed. After 6 h of culture with 500 or 1000 ng/ml BaP, we observed statistically significant increases in the percentages of germ cells with diffuse cytochrome c immunofluorescence, indicative of release into the cytosol, as opposed to punctate, which would indicate mitochondria-localized cytochrome c ($p = .001$, effect of experimental group by Kruskal-Wallis test; Figs. 3C and 3D). Together, these data support and expand on our previous findings to demonstrate that a primary mechanism of BaP-induced germ cell death in the embryonic ovary occurs through DNA damage and subsequent initiation of mitochondrial-mediated apoptosis, resulting in the F1 females being born with fewer oocytes. However, the E13.5 ovary is heterogenous with some oocytes entering meiosis. This led us to question if there is a more sensitive developmental window for exposure to BaP.

Gestational BaP Exposure Hastened Onset of Puberty in F1 Females and Induced Equivalent Germ Cell Depletion Following Exposure During Germ Cell Proliferation or Meiosis Windows

F0 pregnant dams were exposed from either E6.5–11.5 or E12.5–17.5 to assess ovarian developmental sensitivity *in utero* BaP exposure during germ cell proliferation or meiosis I, respectively. F1 females were followed for onset of puberty by assessing vaginal opening and first estrus by vaginal cytology, with onset of puberty being defined as first estrus (Safranski et al., 1993). The results for onset of puberty and estrous cyclicity are in Table 1. We observed that females exposed to BaP during either developmental window had about 2-day earlier onset of puberty than control females ($p = .005$, effect of BaP by GEE); however, there was no statistically significant effect of exposure window or interaction between BaP dose and exposure window. We observed no statistically significant effects on body weight or estrous cyclicity. These data demonstrate that 5-day gestational BaP exposure from E6.5–11.5 or E12.5–17.5 hastens the onset of puberty.

To determine if gestational BaP exposure depletes germ cells differentially during proliferative or meiotic windows, 1 female pup per F0 dam was sacrificed on the day of first estrus, and their ovaries were prepared for histomorphometry. A blinded investigator assessed small follicle counts every fifth section using stereology methods described previously (Luderer et al., 2022; Myers et al., 2004) and large follicles were counted in every section. We observed that gestational BaP exposure resulted in equivalent depletion of primordial (Oil 6.5: 2803 ± 533, Oil 12.5: 3055 ± 886, BaP 6.5: 1138 ± 336, BaP 12.5: 1266 ± 274; $p < .001$, effect of BaP by 2-way ANOVA), primary (Oil 6.5: 366 ± 55, Oil 12.5: 546 ± 163, BaP 6.5: 247 ± 67, BaP 12.5: 289 ± 44; $p = .018$, effect of BaP by 2-way ANOVA), and secondary follicles (Oil 6.5: 99 ± 11, Oil 12.5: 107 ± 12, BaP 6.5: 58 ± 9, BaP 12.5: 62 ± 11; $p < .001$, effect of BaP by 2-way ANOVA), but not antral follicles (Oil 6.5: 11 ± 2, Oil 12.5: 11 ± 1.5, BaP 6.5: 8 ± 1.6, BaP 12.5: 10 ± 1.7) regardless of exposure window (Figure 4). Additionally, we observed no difference in atretic follicle numbers (data not shown). Although there was a slight decrease in healthy antral follicle numbers, it was not statistically significant. This is likely because pubertal ovaries have fewer antral follicles on average, and it is possible that we would see a difference in adult ovaries. These data show that proliferative and meiotic germ cell developmental windows are equally sensitive to BaP-induced germ cell death during F1 ovarian development.

Gestational BaP Oxidatively Damages DNA and Lipids in Pubertal Ovaries and Oocytes

We have demonstrated that BaP gestational and *in vitro* exposure depletes germ cells in F1 pubertal ovaries. To characterize if gestational BaP exposure leads to persistent oxidative damage in F1 pubertal ovaries, we assessed ovarian sections for
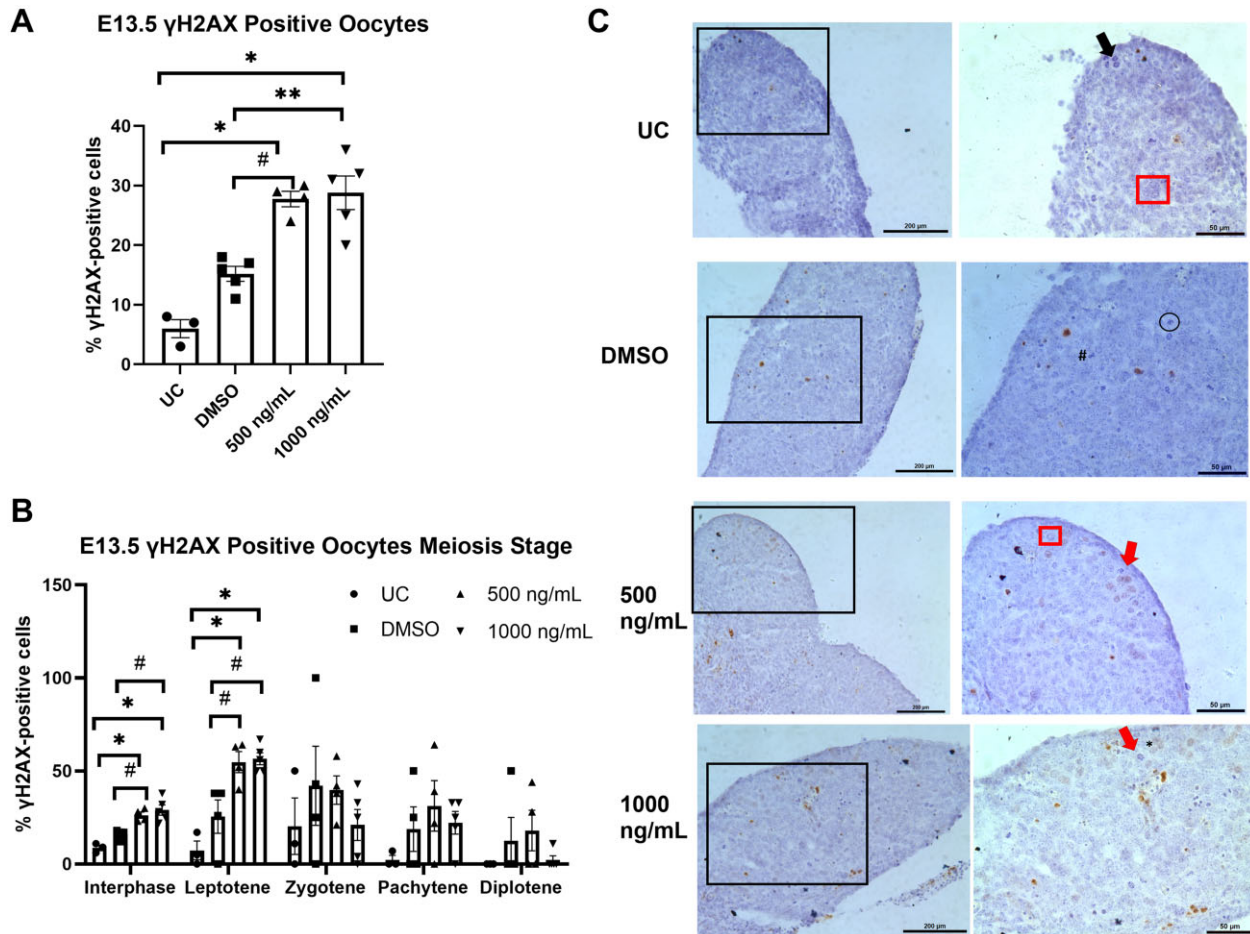
Figure 2. *In vitro* BaP exposure concentration-dependently increases ɣH2AX in germ cells of embryonic ovaries A, Total percent ɣH2AX-positive germ cells per E13.5 ovary increased with BaP concentration following exposure for 6 h ($N = 3$, UC [uncultured]; $N = 4$, DMSO, 500 ng/ml; $N = 5$, 1000 ng/ml. $p = .002$, effect of experimental group by Kruskal-Wallis test. *$p \leq .03$, compared to uncultured, #$p = .014$ and **$p = .009$, compared with DMSO B, Percent ɣH2AX-positive oocytes by meiotic stage per E13.5 ovary increased with BaP dose only in interphase and leptotene oocytes following exposure for 6 h ($N = 3$, UC [uncultured]; $N = 4$, DMSO, 500 ng/ml: $N = 5$, 1000 ng/ml. $p \leq .009$ by Kruskal-Wallis test, effect of experimental group. *$p \leq .05$, compared with uncultured; #$p \leq .05$ compared with DMSO) C, Representative images of ɣH2AX immunohistochemistry. Higher magnification images on right show portions of sections in images on left. Asterisk (*) indicates ɣH2AX-positive oocyte, small square (red in online version) indicates interphase oocyte, black arrow in UC indicates leptotene oocyte, red (online version) arrows in 500 and 1000 ng/mL indicate zygotene oocytes, circle indicates pachytene, and # indicates diplotene. (Scale bars, left panel = 200 μm; scale bars, right panel = 50 μm.) Filled triangles, squares, and circles in the graphs represent individual cultured ovaries.

presence of ovarian ɣH2AX and lipid peroxidation indicated by presence of 4-HNE. 4-HNE is the product from the oxidation of lipids containing polyunsaturated omega-6 acyl groups and is a reliable marker for lipid peroxidation (Dalleau *et al.*, 2013).

We observed borderline statistically significant effects on ovarian histone 2A phosphorylation in the primordial, primary, and secondary follicle oocytes and in primary follicle granulosa cells from exposed females compared with control females ($p = .099$, $p = .046$, $p = .068$, and $p = .097$, respectively by Kruskal-Wallis nonparametric test, Table 2 and Figure 5). Intergroup comparisons revealed that the fraction of ɣH2AX-positive primordial and primary follicle oocytes was decreased in the BaP 12.5 compared with Oil 12.5 ovaries ($p = .010$, $p = .035$, respectively, Mann-Whitney test), and the fraction of ɣH2AX-positive primary follicle oocytes was decreased in the BaP 6.5 compared with Oil 6.5 ovaries ($p = .033$, Mann-Whitney test). Intergroup comparisons revealed that the fraction of primary follicles with ɣH2AX-positive granulosa cells was decreased in BaP 12.5 compared with Oil 12.5 ovaries ($p = 0.035$, Mann-Whitney test). We observed no effect of prenatal BaP on ɣH2AX in antral follicles.

To test whether BaP exposure *in utero* results in persistent oxidative lipid damage in the ovary, we performed immunostaining with an antibody against 4-HNE and found that prenatal BaP exposure during both exposure windows increased lipid peroxidation levels in pubertal ovaries ($p < .05$, effect of BaP, GEE; Figs. 6A and 6B). However, we saw no change in the neutral lipid content across all treatment groups (Figs. 6C and 6D). These data show that gestational BaP exposure results in persistent oxidative damage in F1 ovaries in the form of ovarian lipid peroxidation regardless of exposure window.

Gestational BaP Exposure Alters Mature F1 Oocyte Quality Through Increased Oxidative Stress and Decreased Lipid Droplet Content

Previous studies have shown that lipids, more specifically LDs, and their metabolism play a significant role in determining mature oocyte quality (Paczkowski *et al.*, 2014; Valsangkar and Downs, 2013) and that oocyte LD content is regulated by the surrounding granulosa and cumulus cells, as well as the follicular fluid (Zhang *et al.*, 2020). We were interested in exploring how the increased lipid peroxidation in BaP6.5 ovaries affected
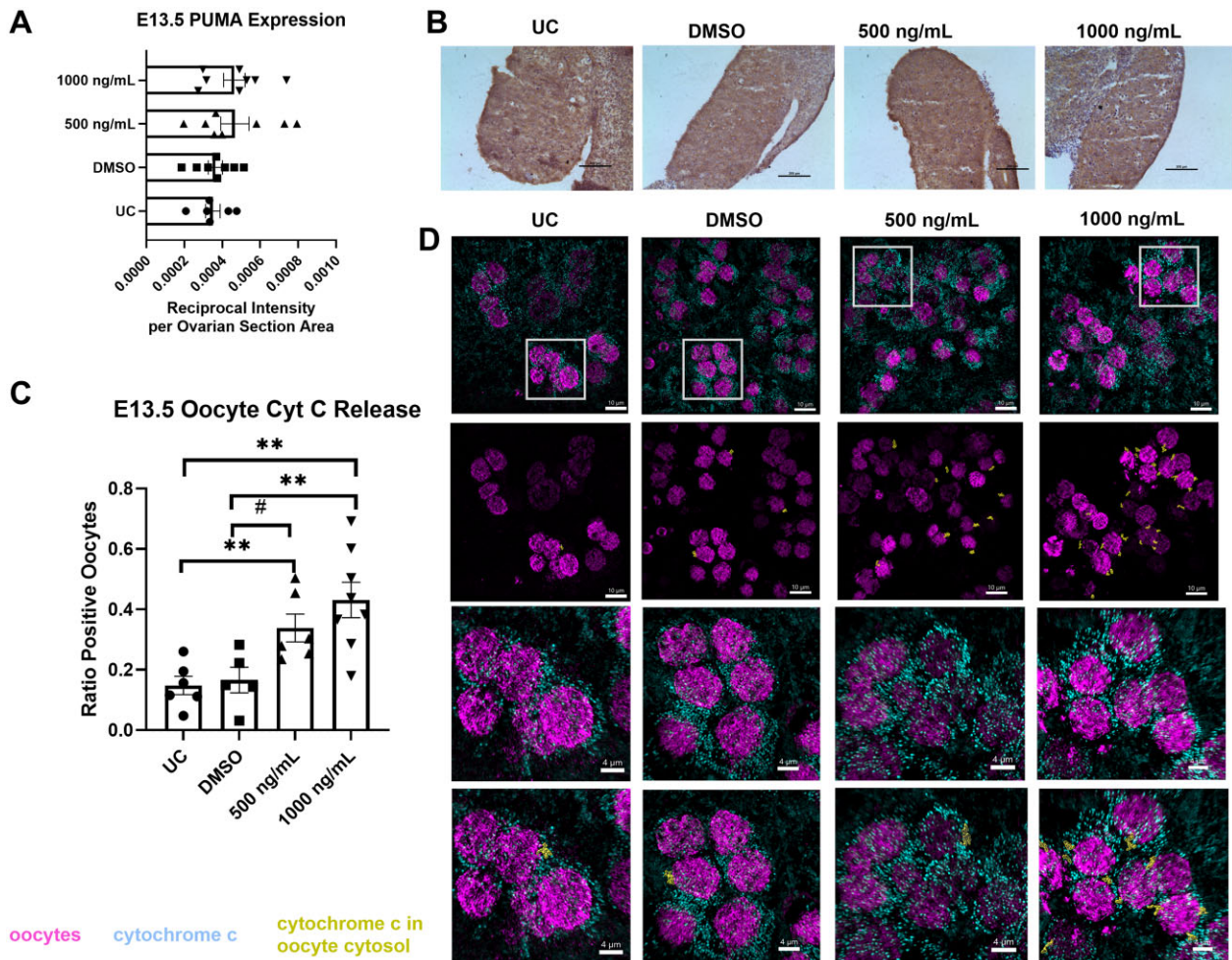
Figure 3. *In vitro* BaP exposure for 6 h had no effect on PUMA protein expression but dose-dependently increased cytochrome c release in exposed ovaries. A, Reciprocal intensity per ovarian section area was estimated in E13.5 ovaries and showed a slight, but not statistically significant, increase in PUMA immunostaining in the whole ovary ($N = 6$, UC [uncultured]; $N = 8$, DMSO, 500 ng/ml, 1000 ng/ml). B, Representative images of PUMA immunohistochemistry show ubiquitous and similar expression regardless of exposure. C, Cytochrome C release from the mitochondria in germ cells following BaP exposure was measured using immunofluorescence. Methods for analysis of images to estimate the ratio of oocytes positive for cytochrome c release are detailed in the Materials and Methods. These results show a dose-dependent increase in the ratio of positive oocytes ($N = 6$, UC; $N = 5$, DMSO; $N = 6$, 500 ng/ml; $N = 8$, 1000 ng/ml. $p = .001$, effect of experimental group, Kruskal-Wallis test. **$p \leq .008$, compared with DMSO or uncultured; #$p = .045$ compared with DMSO, Mann-Whitney test). D, Representative images of immunofluorescence. Top row shows germ cell-specific nuclear marker GCNA (magenta in online version) and cytochrome c (smaller dots surrounding oocyte nuclei; cyan blue in online version). Second row shows Imaris analysis with GCNA (oocyte nucleus, magenta in online version) and cytochrome c in oocyte cytosol (smaller fluorescent areas; yellow in online version), scale bars = 10 μm. Third row and 4th rows show same as top and second rows, respectively zoomed in, scale bars = 4 μm. Filled triangles, squares, and circles in the graphs represent individual cultured ovaries.

Table 1. Effects of Gestational BaP on F1 Age at Puberty and Estrous Cyclicity

Treatment	N	Age at Puberty Onset (PND)*	Body Weight at Puberty Onset (g)	Mean ± SEM Cycle Length (Days)	Mean ± SEM % Days with Leukocytic Cytology	Mean ± SEM % Days with Cornified Cytology
Oil 6.5	8	36.9 ± 1.5	15.8±0.4	4.3 ± 0.08	43.4 ± 2.6	26.7 ± 1.1
Oil 12.5	5	38.5±0.6	16.4±0.2	4.4 ± 0.07	42.5 ± 3.1	39.1 ± 4.1
BaP 6.5	9	36.2±0.7	16.2±0.3	4.6 ± 0.21	40.7 ± 4.6	40.6 ± 6.1
BaP 12.5	12	35.2 ±1.0	16.4±0.4	4.7 ± 0.53	35.0 ± 7.0	50.5 ± 9.7

*$p = .006$, effect of BaP, GEE. N refers to the number of F0 dams per treatment for puberty. N for estrous cycle was 5–7 F0 dams/group and estrous cycling was examined in F1 females at 5–7.5 months of age.

mature oocyte LD content and ovulated oocyte oxidative state. The BaP6.5 window was chosen because we had observed no differences in effects on ovarian follicle counts or oxidative lipid damage between the 2 exposure windows.

BaP 6.5 and Oil 6.5 pubertal females were superovulated and their morphologically healthy, mature oocytes were assessed for indications of oxidative stress. We examined only morphologically healthy oocytes because we were interested in whether
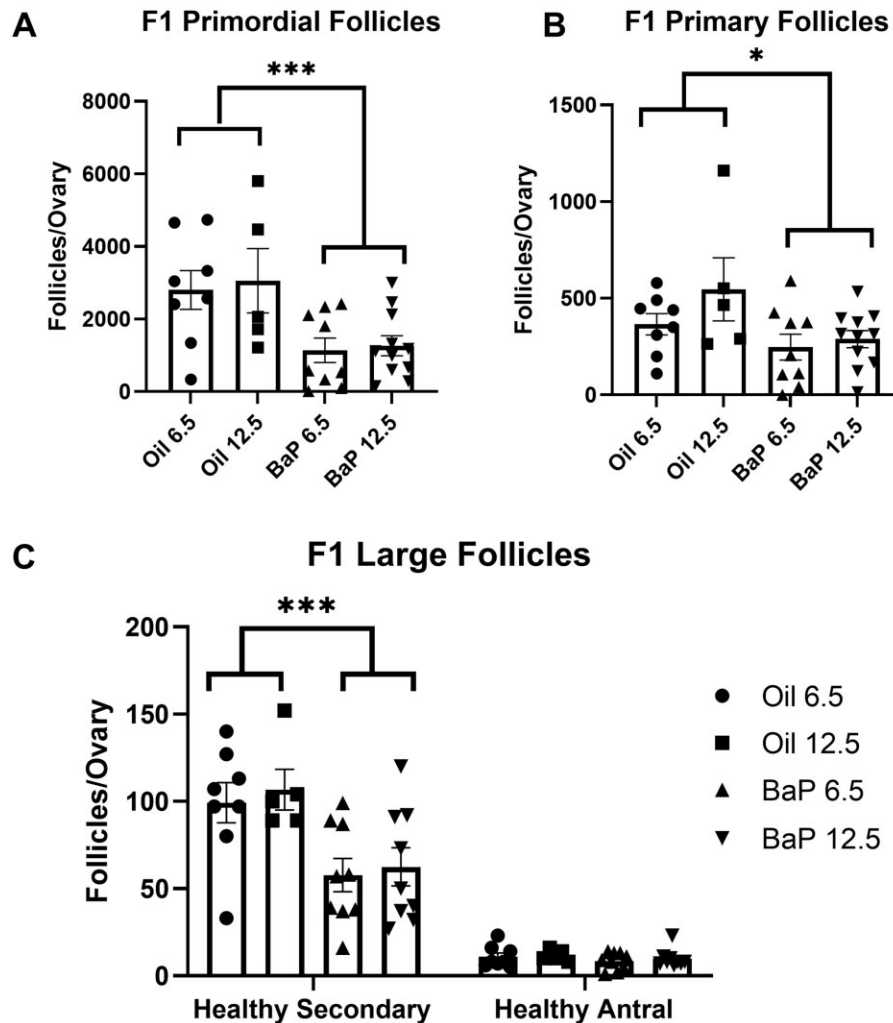
Figure 4. Gestational BaP exposure decreased primordial, primary, and secondary follicles in F1 pubertal ovary regardless of exposure window (E6.5–11.5 or E12.5–17.5). Total number of primordial (A), primary (B), and secondary (C) follicles in the F1 ovaries on 1st estrus were significantly decreased following BaP exposure during both developmental windows, but no difference in the total number of antral follicles (C) was observed. ($N = 8$ F0 dams, Oil 6.5; $N = 5$ Oil 12.5; $N = 9$, BaP6.5; $N = 10$, BaP12.5, ***$p < .001$, *$p < .05$, effect of BaP treatment by 2-way ANOVA.) Filled triangles, squares, and circles in the graphs represent data from individual mice.

Table 2. Effects of Gestational BaP Exposure on Ovarian γH2AX Immunostaining at Puberty

	% Follicles With Positive Granulosa Cells			% Follicles With Positive Oocytes			
	Primary ± SEM[a]	Secondary ± SEM	Antral ± SEM	Primordial ± SEM[b]	Primary ± SEM[c]	Secondary ± SEM[d]	Antral ± SEM
Oil 6.5	11 ± 5	72 ± 5	50 ± 29	60 ± 6	82 ± 6	74 ± 5	50 ± 29
Oil 12.5	22 ± 7	47 ± 14	57 ± 8	64 ± 3	84 ± 10	35 ± 9	37 ± 12
BaP 6.5	8 ± 3	47 ± 10	64 ± 11	46 ± 10	45 ± 15*	50 ± 12	51 ± 13
BaP 12.5	4 ± 3*	63 ± 7	47 ± 18	47 ± 4*	61 ± 9*	62 ± 11	33 ± 17

$N = 4$, Oil 6.5; $N = 5$, Oil 12.5; $N = 6$, BaP 6.5 and BaP 12.5.
[a]$p = .097$.
[b]$p = .099$.
[c]$p = .046$.
[d]$p = .068$, effect of experimental group, Kruskal-Wallis.
*$p < .05$ versus Oil same dosing window, Mann-Whitney test.

these apparently healthy oocytes might have subcellular abnormalities that could adversely impact fertilization and/or early embryonic development. There were no statistically significant differences in number of healthy MII oocytes ovulated between treatment groups (Oil 6.5: 13.7 ± 2.5, BaP 6.5: 10.9 ± 2.7, $N = 9$

litters/treatment). We measured mitochondrial superoxide production using MitoSOX and we observed a significant increase in superoxide production in oocytes of BaP6.5 females compared with Oil 6.5 ($p = .006$, GEE, Figure 7A). Intriguingly, discordant with the increase in lipid peroxidation in BaP 6.5 ovaries, we
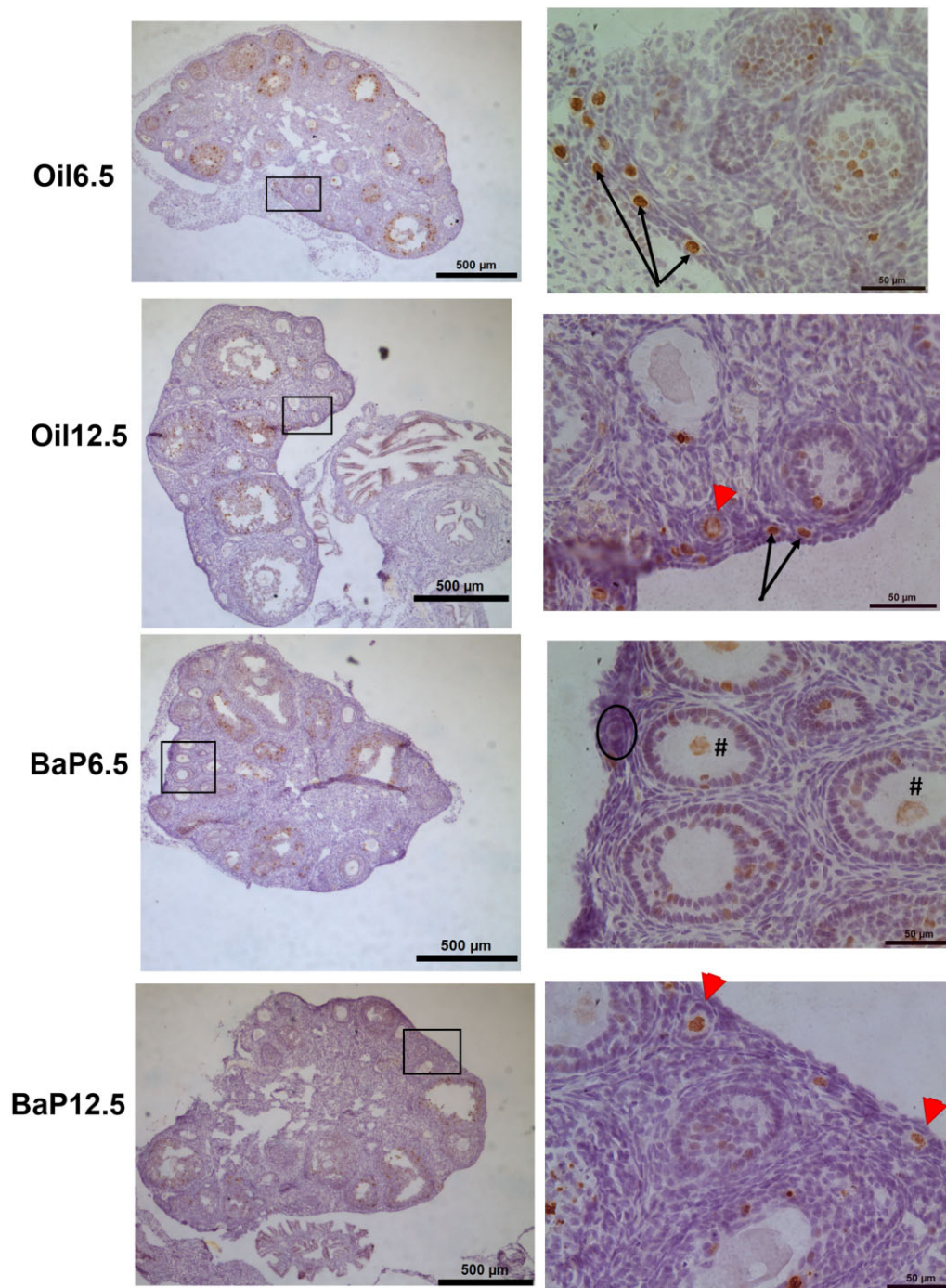
Figure 5. Representative images of ɣH2AX IHC in F1 pubertal ovaries. ɣH2AX is the brown staining. Left panel images taken with a 10× objective. Right panel images of areas shown by rectangles in left images taken with a 40× objective. Black arrows point to positive primordial oocytes, arrowheads point to positive primary oocyte, oval encompasses a negative primordial follicle, # indicates positive secondary follicle and oocyte. (Scale bar, left panel = 500 μm; scale bar, right panel = 50 μm.)

observed no difference in lipid peroxidation in the mature oocytes between treatment groups, measured as oxidized: unoxidized lipid ratio (Oil 6.5: 2.05 ± 0.05, BaP 6.5: 1.92 ± 0.37, $N = 3$ females/treatment). Nor did we observe differences in whole oocyte GSH levels between treatment groups, measured by monochlorobimane fluorescence (Oil 6.5: 57 705.7 ± 4572.9, BaP 6.5: 56 945.01 ± 771.1, $N = 3$ females/treatment). Together, these data suggest that gestational BaP exposure results in

persistent oxidative stress in the mitochondria but has no effect on the oxidation state of lipids in the mature oocyte.

To further explore indicators of mitochondrial oxidative stress, we assessed mitochondrial membrane potential ($\Delta\Psi$m) in the whole oocyte. Using the fluorescent probe, JC-1, we observed a statistically significant decrease in $\Delta\Psi$m in BaP6.5 oocytes compared with Oil 6.5 ($p = .04$, GEE; Figs. 7B and 7C). Membrane potential in the mitochondria is created by the
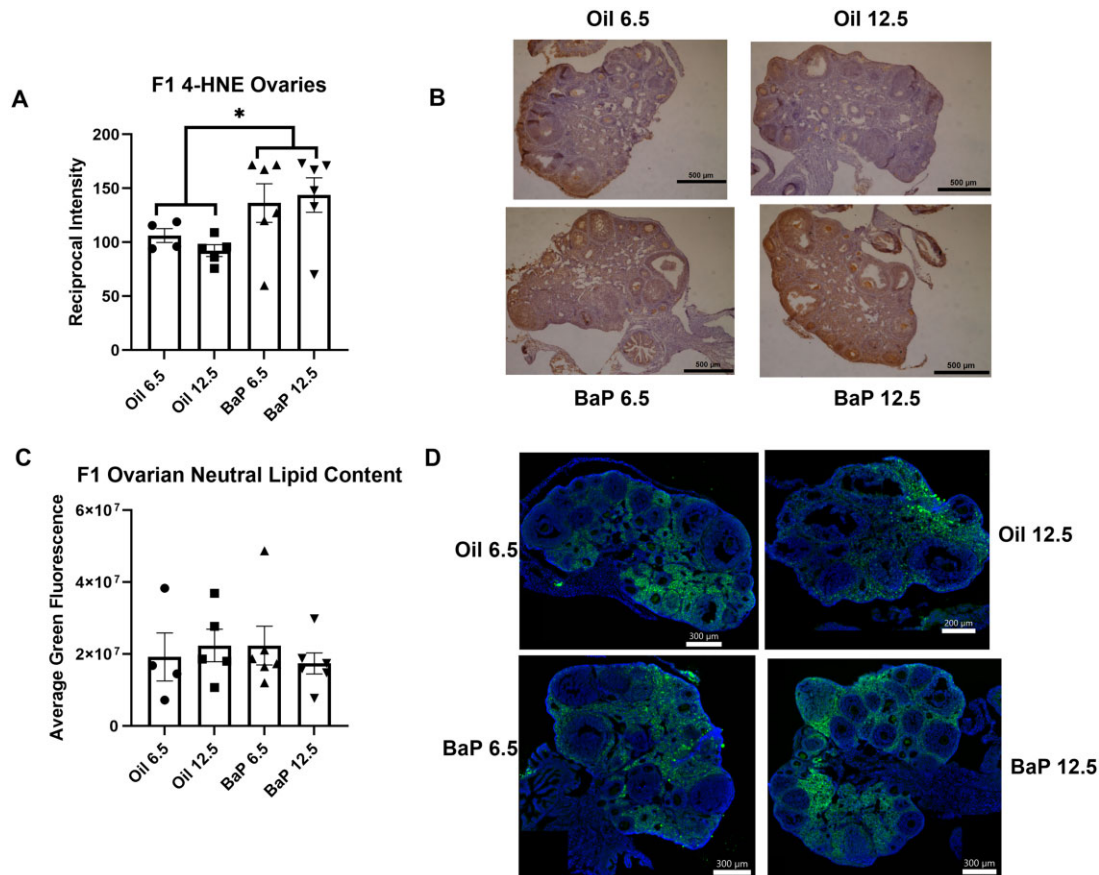
Figure 6. Gestational BaP exposure results in persistent oxidative stress in F1 ovaries but has no effect on ovarian neutral lipid content. A, 4-HNE immunostaining intensity estimated per total ovarian section area using reciprocal intensity shows persistently increased lipid peroxidation following gestational exposure regardless of exposure window ($N = 4$–5 F0 dams, oil treatment; $N = 6$ F0 dams, BaP treatment, $*p < .05$, effect of BaP by 2-way ANOVA). B, Representative 4-HNE immunostaining (brown color in online version). C, Quantification of neutral lipid content in ovarian sections stained with BODIPY 493/503 showed no treatment or exposure window-related differences in neutral lipid content. D, Representative images of BODIPY 493/503 sections, counterstained with DAPI. Neutral lipids fluoresce green (online version). Filled circles, squares, and triangles represent data from individual mice.

pumping of protons across the inner membrane by the Complexes I, III, and IV of the electron transport chain. Complexes I and III are primary sources of superoxide; therefore, decreased $\Delta\Psi$m further supports that gestational BaP exposure resulted in increased mitochondrial oxidative stress. Additionally, we observed no difference in oocyte mitochondrial content between the 2 treatments (Figure 7D), affirming that any changes in $\Delta\Psi$m did not result from a decrease in mitochondria following exposure. Additionally, we interrogated differences in mitochondrial clustering patterns in BaP-exposed and control oocytes to further our understanding of the oocyte oxidative stress response. We observed no significant effect of BaP on mitochondrial clustering (Figure 7E).

ROS, including superoxide, react stochastically with the first molecules they contact, thus oxidizing them. Mitochondria are often found to be colocalized with LDs (Benador et al., 2018; 2019), therefore we found it curious that despite increased superoxide production and decreased $\Delta\Psi$m, there were no observable changes in lipid peroxidation in BaP6.5 oocytes. To this end, we assessed neutral lipid content and mitochondria: LD colocalization in these oocytes. Using the neutral lipid stain, BODIPY 493, we observed that average LD volume in BaP 6.5 oocytes was significantly smaller compared with Oil 6.5 ($p < .001$, effect of BaP, GEE; Figs. 8A and 8C). To characterize mitochondria: LD colocalization, we used Mitotracker Deep Red

and BODIPY 493. We observed that even though there was no difference in mitochondria content between BaP and control oocytes (Figure 7D), BaP6.5 oocytes had borderline significantly decreased proportion of mitochondria colocalized with LDs compared with Oil 6.5 ($p = .075$, GEE; Figs. 8B and 8C), and the LDs colocalized with the mitochondria were statistically significantly smaller in volume in exposed oocytes ($p < 0.001$, GEE; Figs. 8A and 8C). Together, these data show that BaP exposure *in utero* increases mitochondrial oxidative stress and decreases LD content in mature F1-derived oocytes.

DISCUSSION

We observed a significant increase in ɣH2AX-positive oocytes, a nonsignificant increase in ovarian expression of the proapoptotic BCL-2 family member PUMA, and a significant increase in oocytes positive for cytochrome c release, a key event in the intrinsic or mitochondrial apoptotic pathway, in E13.5 ovaries cultured with BaP. *In utero* exposure to BaP at 2 mg/kg/day hastened the onset of puberty in F1 females and resulted in equivalent depletion of healthy primordial, primary, and secondary follicles regardless of prenatal mitotic or meiotic exposure window. Expression of the lipid peroxidation marker 4-HNE was also significantly increased in both BaP6.5 and BaP12.5 F1 pubertal ovaries compared with Oil controls. Interestingly, in contrast
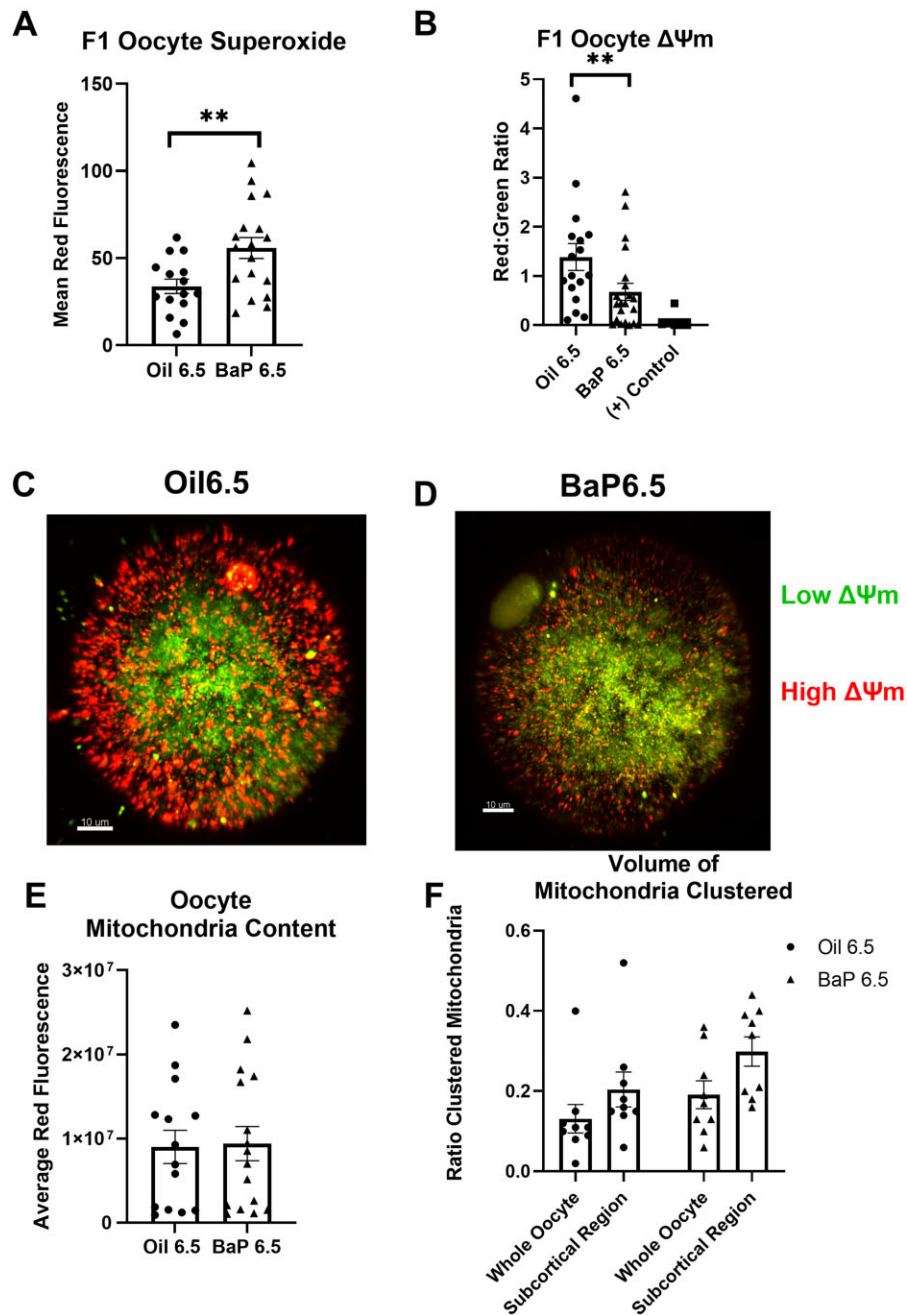
Figure 7. Gestational BaP exposure results in persistent oxidative stress in F1-derived superovulated MII oocytes. A, Mean red fluorescence intensity of MitoSOX demonstrates increased mitochondrial superoxide anion in oocytes of females exposed to BaP during the proliferative developmental window from E6.5–11.5 ($N = 9$ F0 dams, Oil; $N = 8$ F0 dams, BaP; **$p = .006$, effect of BaP by GEE). B, Mitochondrial membrane potential ($\Delta\Psi m$), measured using JC-1 shows that oocytes of females exposed to gestational BaP during the proliferative developmental window have reduced $\Delta\Psi m$ compared with oocytes from oil control females. Positive control oocytes were exposed to $1\,\mu M$ of CCCP (carbonyl cyanide 3-chlorophenylhydrazon), a known mitochondrial uncoupler, which breaks down the $\Delta\Psi m$ ($N = 8$ F0 dams, Oil; $N = 9$ F0 dams, BaP; $N = 5$; positive control; *$p = .04$, effect of BaP by GEE). (C, D) Representative images of $\Delta\Psi m$ from control (C) and BaP (D) exposed mice (red= high $\Delta\Psi m$, green= low $\Delta\Psi m$, colors in online version; scale bar= $10\,\mu m$). E, Mitochondrial content of MII oocytes estimated by red fluorescence of Mitotracker Deep Red was not affected by prenatal BaP treatment ($p = .17$, effect of BaP, ANOVA with oocyte as random effect. F, Ratio of clustered mitochondrial volume in whole oocyte and subcortical region was not affected by prenatal BaP treatment ($N = 9$ F0 dams/treatment, $p > .50$, effect of BaP, GEE). Individual data points for (A), (B), (E), and (F) represent measurements from individual oocytes.

to the E13.5 ovary, F1 pubertal ovaries had significantly (primary follicle oocytes) or borderline significantly decreased ɣH2AX-positive primary follicle granulosa cells and primordial and secondary follicle oocytes. Gestational BaP exposure during the mitotic window resulted in oocytes with decreased average LD volume, mitochondria: LD colocalization, and $\Delta\Psi m$ and increased mitochondrial superoxide levels compared with control oocytes.

Together with our previously published data (Lim et al., 2016; Lim and Luderer, 2018), the current data demonstrate that BaP-induced germ cell death in the developing ovary is mediated through the mitochondrial apoptosis pathway. A myriad of
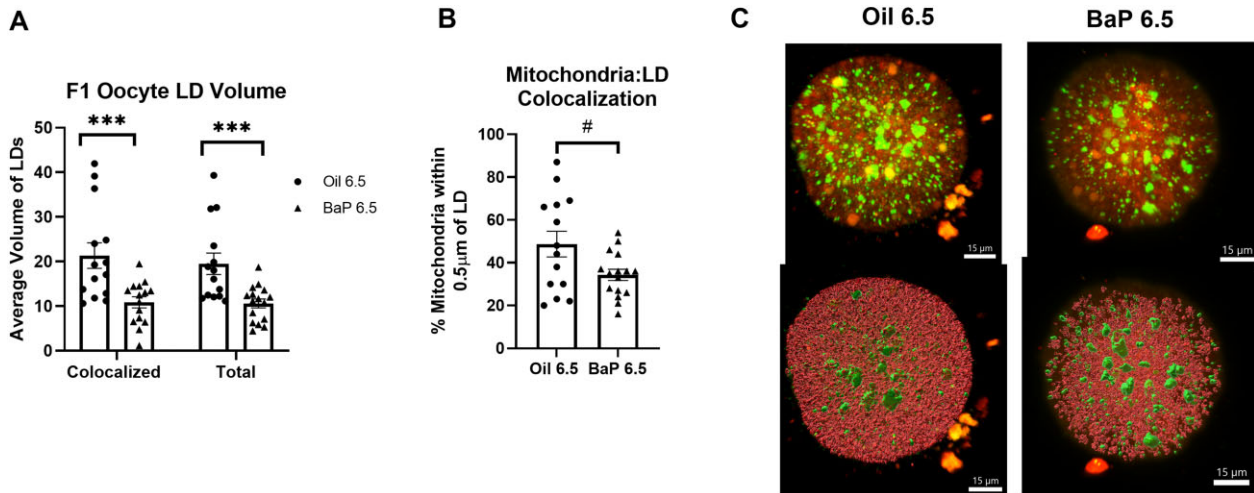
Figure 8. Gestational BaP exposure significantly decreases oocyte LD content. A, Average volume of a single LD in the whole oocyte and in the subpopulation colocalized with mitochondria, estimated using Imaris imaging software to build 3D volumes from 3D rendered z-stack images, is significantly decreased in oocytes from females exposed to BaP during E6.5–11.5 ($N = 9$ F0 dams/group, ***$p < .001$, effect of BaP by GEE). B, Estimation of the percent of mitochondria colocalized with LDs estimated using Imaris to generate 3D volumes. Mitochondrial volumes within 0.5 μm of an LD volume were considered to be colocalized with LDs. Colocalization of mitochondria with LDs is decreased in gestationally exposed oocytes ($N = 9$ F0 dams/treatment #$p = .075$, effect of BaP by GEE). Individual data points for (A), (B) represent measurements from individual oocytes. C, Representative images of Mitotracker Deep Red (red in online version) and BODIPY 493/503 (green in online version) co-staining in oocytes (top panel). Representative images of Imaris volume renderings (bottom panel).

signals can induce activation of this pathway including, but not limited to, oxidative stress and DNA damage. In the present study, we observed an increase in the marker for DNA DSBs, ɣH2AX, in the germ cells of E13.5 ovaries cultured with BaP for 6 h (Figure 2). Some oogonia begin to progressively enter meiosis at E13.5, after completing their migration to the gonadal ridge; therefore, each ɣH2AX-positive oocyte was categorized by meiosis stage. Chromosomal crossover occurs during the pachytene stage of meiosis I; we observed no differences in the percentages of ɣH2AX-positive oocytes among any of the treatment groups in the pachytene stage. Instead, a significant increase in ɣH2AX-positive oocytes in interphase and leptotene stages was observed (Figure 2B). These data show that BaP significantly increases DNA DSBs in oocytes, possibly due to increased oxidative stress. DNA damage is known to induce the mitochondrial apoptosis pathway. Our previous work showed that embryonic ovaries were more sensitive than the embryonic testis to BaP-induced germ cell death and that this cell death was likely mediated through the mitochondria with a concentration-dependent increase in BAX at 6 h and cleaved caspase-9 and -3 at 24 h in culture (Lim et al., 2016). Additionally, in a subsequent study, we observed that cultured embryonic ovaries deficient in the antioxidant glutathione were more sensitive to BaP-induced oocyte death than wildtype embryonic ovaries (Lim and Luderer, 2018).

In the current study, we assessed E13.5 ovaries for PUMA (also known as BCL2-binding component 3, BBC3) protein expression. PUMA protein is diffusely present in the E13.5 ovary, and its deletion increases the size of the germ cell pool at E13.5 and of the primordial follicle pool at PND 10 (Myers et al., 2014). As a pro-apoptotic BH3-only BCL2 family protein, PUMA inhibits the anti-apoptosis regulator BCL-2, thus allowing for the formation of BAX pores in the mitochondria, which triggers the release of cytochrome c into the cytosol (Han et al., 2001; Nakano and Vousden, 2001). PUMA is required for induction of germ cell apoptosis in the PND 5 mouse ovary by ionizing radiation exposure (Kerr et al., 2012); therefore, we hypothesized that it might play a role in BaP-induced germ cell apoptosis in the

prenatal ovary. BaP exposure slightly increased the expression of PUMA regardless of dose after 6 h (Figs. 3A and 3B). The observation of a slight, but nonsignificant, increase in PUMA expression in BaP-exposed ovaries could be attributed to the timing of exposure; it is possible that an earlier timepoint could have captured a significant increase in PUMA expression in response to BaP exposure. BAX-dependent cytochrome c release is primarily dependent on the concentration of BAX and not on time. Release of cytochrome c has been detected as early as 5 min after BAX channel formation (Eskes et al., 1998). To confirm that BaP exposure does lead to mitochondrial-mediated apoptosis, we performed immunofluorescence to assess cytochrome c release in germ cells. We observed a statistically significant, dose-dependent increase in the percentage of germ cells positive for cytochrome c release, determined by diffuse as opposed to punctate fluorescence signal (Feng et al., 2012; Liu et al., 2003), in E13.5 ovaries exposed to both 1000 and 500 ng/ml of BaP for 6 h compared with DMSO and uncultured controls (Figs. 3C and 3D). Together, these data extend previous findings (Lim et al., 2016; Lim and Luderer, 2018; Matikainen et al., 2002), with compelling evidence, that a primary driver of BaP-induced germ cell death is DNA damage, resulting in activation of mitochondrial apoptosis in the embryonic ovary. The germ cell population in the E13.5 ovary is made up of proliferating germ cells as well as germ cells entering meiosis, therefore these data provide compelling evidence that mitochondrial apoptosis is a primary driver of BaP-induced germ cell death. However, what is left unanswered by these data is whether there is a more sensitive window of germ cell development to BaP-induced cell death. To answer this question, we used an in utero study.

We previously showed that exposure in utero to 2 mg/kg/day of BaP from E6.5–15.5 hastened the onset of puberty by about 5 days, determined by age at first estrus in comparison with oil controls (Luderer et al., 2017). Additionally, BaP exposure to 2 and 10 mg/kg/day in utero during this same developmental window resulted in decreased primordial, primary, and secondary follicles in peripubertal and adult F1 females (Lim et al., 2013; Luderer et al., 2017). This gestational exposure window includes

2 very distinct germ cell populations. From E7 to E11.5, germ cells proliferate rapidly before and while migrating along the hindgut mesentery to reach the bipotential gonadal ridge. The germ cells continue their rapid proliferation until entering meiosis, beginning at E13.5 (Findlay et al., 2015; Wear et al., 2016). Recently, we have shown that both the mouse embryo and placenta are capable of metabolizing BaP, in a sex and dose-dependent manner with female embryos and placentas generating higher metabolite concentrations (ng/g) compared with male embryos following gestational exposure from E6.5–11.5 to 0, 0.2, or 2 mg/kg/day (Lim et al.,, 2022). What was not explored in the previous studies was whether one of these distinct germ cell populations was more sensitive to BaP-induced germ cell death than the other. To assess this, we broke up the previous exposure windows into 2 developmental windows, E6.5–11.5 (proliferative) and E12.5–17.5 (meiotic). Our data show that BaP exposure during either developmental window, proliferative or meiotic, hastens the onset of puberty (Table 1). Exposure to estradiol (Biegel et al., 1998) and the xenoestrogen methoxychlor (Chapin et al., 1997) in utero results in earlier onset of puberty. Others have shown that BaP metabolites are capable of binding estrogen receptors (Plíšková et al., 2005, van Lipzig et al., 2005). Therefore, we hypothesize that the mechanism by which BaP exposure in utero results in earlier pubertal onset involves estrogen receptor signaling.

Additionally, we observed that gestational BaP exposure, regardless of exposure window, decreased primordial, primary, and secondary follicle numbers, but had no effect on antral or atretic follicles at first estrus (Figure 4 and data not shown). In view of the rapid metabolism of BaP and decline in concentrations of its metabolites in plasma and tissues of offspring to undetectable levels within the first post-natal month after prenatal dosing (Ramesh et al., 2001, Wu et al., 2003, Jules et al., 2012) and our above-mentioned studies demonstrating germ cell death in embryonic ovaries exposed to BaP, we conclude that the reduced follicle numbers post-natally are due primarily to prenatal germ cell destruction. However, our findings in the present study of persistent ovarian oxidative lipid damage and DNA damage raise the possibility that chronic oxidative stress due to prenatal BaP exposure may also cause ongoing post-natal follicle loss.

Contrary to our hypothesis, we observed decreased granulosa cell and/or oocyte histone 2AX phosphorylation, a marker for DNA DSBs, in primordial and primary follicles of mice exposed in utero to BaP at first estrus compared with controls (Table 2 and Figure 5). A recent study using ɣ-irradiated wild-type and apoptosis-deficient mice, found primordial oocytes were highly efficient in repair of DNA DSBs preferentially relying on homologous recombination, reporting a statistically significant increase in ɣH2AX-positive primordial oocytes following ɣ-irradiation of PND 10 females at 0.1, 0.2, 0.45, 4.5, or 7 Gy (Stringer et al., 2020). This same study also reported a statistically significant increase in pATM and RAD51 in primordial oocytes following irradiation (Stringer et al., 2020). Our group has shown that heavy ion irradiation increased ovarian 4-HNE, PUMA, and activated caspase 3, resulting in follicle depletion in adult mice (Mishra et al., 2016, 2017). Both studies also documented that irradiation induced DNA DSBs and increased ɣH2AX at 6 h post-exposure (Mishra et al., 2016, 2017). In the present work, we observed a similar increase in ɣH2AX-positive germ cells in embryonic ovaries cultured for 6 h with BaP but decreases in ɣH2AX-positive follicles at puberty. We postulate that a combination of prenatal BaP-induced apoptotic clearance of damaged germ cells combined with induction of DNA repair

resulted in the decreased percentages of ɣH2AX-positive oocytes in primordial and primary follicles observed at the pubertal time point.

We observed a statistically significant increase in the lipid peroxidation marker 4-HNE in F1 pubertal ovaries, following exposure during both windows (Figs. 6A and 6B). We have previously shown that glutathione-deficient mice show an accelerated age-related decline in ovarian follicles and increased lipid peroxidation measured as immunostaining for 4-HNE compared with their wildtype littermates (Lim et al., 2015). We were surprised to observe equivalent effects of BaP during both exposure windows, but it is worth addressing that developing germ cells progressively begin to enter meiosis starting on E13.5 while many germ cells are still proliferating (Findlay et al., 2015; Wear et al., 2016). Progressive entry into meiosis in response to retinoic acid signaling from the mesonephros creates a heterogenous population of meiotic and proliferative germ cells (Koubova et al., 2006), making it virtually impossible to fully distinguish exclusively mitotic and exclusively meiotic germ cell populations by exposure window. Therefore, it is possible that the equivalent effect of BaP on lipid peroxidation and follicle depletion during both exposure windows is due to BaP affecting primarily proliferating germ cells during both windows.

Lastly, we explored whether gestational BaP exposure altered oocyte developmental competence in F1 females. Other groups have characterized oxidative stress in the oocytes of female mice following maternal (Sui et al., 2020) and neonatal (Sobinoff et al., 2012) BaP exposure. Sui et al. orally dosed F0 females with 0 or 40 mg/kg/day of BaP in corn oil for 10 days prior to mating. F1 females were superovulated for mature oocytes. They observed that BaP significantly reduced germinal vesicle break down and polar body extrusion (Sui et al., 2020). Further they reported significantly decreased fluorescence intensity of Mitotracker staining, decreased ATP production, and increased ROS production in exposed oocytes. We observed a significant decrease of $\Delta\Psi$m in oocytes of females exposed to BaP from E6.5–11.5 (Figs. 7B and 7C), accompanied by a significant increase in mitochondrial superoxide production (Figure 7A) compared with oocytes from control females. Oxidative phosphorylation and the electron transport chain are the primary sources of superoxide and ROS in the cell (Guérin et al., 2001). Complexes I, III, and IV pump protons into the intermembrane space as they transfer electrons from electron donors to acceptors thus creating $\Delta\Psi$m. Complexes I and III are sources of mitochondrial superoxide. Together these data suggest that gestational BaP exposure induces mitochondrial oxidative stress in the F1-derived oocytes, leading to a compensatory decrease in $\Delta\Psi$m to avoid further ROS generation. In contrast to Sui et al., we did not observe a difference in fluorescence intensity of Mitotracker in the oocytes derived from females exposed to BaP from E6.5–11.5 (Figure 7D). This is likely the result of using a much lower dose and different dosing window compared with Sui et al., who used a dose 20 times higher than the one in the current study with preconception dosing.

Sobinoff et al. exposed PND 4 females to a dosing regimen more comparable with ours of 0, 1.5, and 3 mg/kg/day of BaP in sesame oil for 7 days and superovulated the F1 females at 6 weeks old (Sobinoff et al., 2012). They observed a significant increase in mitochondrial superoxide and lipid peroxidation in oocytes at both 1.5 and 3 mg/kg/day (Sobinoff et al., 2012). Our data show that gestational BaP exposure increases mitochondrial superoxide, whereas having no effect on lipid peroxidation. The doses used in these studies are comparable. However,

our study used a gestational dosing paradigm, whereas the Sobinoff *et al.* study exposed neonatal mice (Sobinoff et al., 2012), leading us to conclude that timing of BaP exposure may modulate the impact of BaP on lipid peroxidation in mature oocytes. We have previously shown that prenatal BaP exposure accelerates age-related ovarian decline (Lim et al., 2013), and others have demonstrated that oocytes exposed to BaP *in vitro* and *in vivo* show signs of decreased developmental competence such as increased incidence of meiotic spindle abnormalities (Zhang et al., 2018), increased ROS (Sui et al., 2020), decreased sperm fusibility (Sobinoff et al., 2012), and increased incidence of aneuploidy (Li et al., 2019)—all of which are accepted signs of aged oocytes (Bianchi et al., 2015; Kushnir et al., 2012). Therefore, it is possible that following gestational exposure, the lipids in an oocyte will slowly undergo peroxidation as the female ages, due to persistent oxidative stress in the ovary and oocyte, as evidenced by increased 4-HNE and mitochondrial superoxide, respectively.

We previously reported that glutathione-deficient oocytes have increased oxidative stress, but not increased lipid peroxidation (Malott et al., 2022). We concluded that a possible reason for this was the observed decreased LD content in glutathione-deficient oocytes (Malott et al., 2022). Interestingly, we observed a similar effect of gestational BaP exposure on average LD volume in oocytes (Figs. 8A and 8C), with oocytes of females exposed to BaP from E6.5–11.5 possessing smaller LDs by volume compared with oocytes of control females. LDs have been shown to be of great importance to preimplantation embryonic development (Bradley and Swann, 2019; Collado-Fernandez et al., 2012; Dunning et al., 2010). Delipidated mature oocytes begin producing new LDs through *de novo* lipogenesis almost immediately, further supporting the significant role that LDs play in oocyte competence (Aizawa et al., 2019). Lipids in the oocytes are stored throughout oogenesis from a combination of sources including *de novo* synthesis (Aizawa et al., 2019), from granulosa cells (Dunning et al., 2014), and from the follicular fluid which is supplied predominantly from serum (Zhang et al., 2020). BaP exposure has previously been shown to alter lipid metabolism in mice. In a study by Li *et al.*, a single 5 μl dose at 5 mg/ml of BaP in corn oil was administered to mice at the bronchial bifurcation through tracheal instillation (Li et al., 2020). Liver homogenates were analyzed from mice 1, 3, 7, and 21 days post-dosing using UHPLC-HRMS, and it was observed that BaP exposure significantly altered hepatic lipid classes with decreased phosphotidylethanolamines, lysophospholipids, free fatty acids, and eicosanoids, and increased phosphotidylinositols, phosphotidylcholines, and triacylglycerols (Li et al., 2020). Triacylglycerols were reported to be the most sensitive to BaP exposure, with their hepatic content increasing 2.2-fold in the first day following exposure, suggesting that BaP exposure significantly increases hepatic triacyglycerol synthesis (Li et al., 2020). Other studies have demonstrated that activation of the aryl-hydrocarbon receptor induces differential regulation of lipid synthesis following exposure (Hu et al., 2016a,b; Neuschäfer-rube et al., 2015). These data collectively support the dysregulation of LD storage in the oocyte following gestational BaP exposure.

To further understand the interplay between oocyte mitochondrial oxidative stress and LDs in the oocyte, we analyzed mitochondria: LD colocalization. In the current study, we observed that gestational BaP exposure decreased, approaching statistical significance, the percentage of mitochondria that were colocalized with LDs and further, the colocalized LDs were statistically significantly smaller by volume (Figs. 8A and 8C).

There is still much to discover about the role of LDs in all cell types, especially in oocytes. Mitochondria colocalized with LDs are referred to as peridroplet mitochondria and depending on the cell type, it is accepted that peridroplet mitochondria can either be lipid consuming (fatty acid β-oxidation) or lipid synthesizing (lipogenesis) (Benador et al., 2018; 2019). It is currently not well understood which category peridroplet mitochondria in mature oocytes fall under; therefore, the implications of the present findings remain unclear. Mature oocytes are predominantly dependent on fatty acid β-oxidation and pyruvate oxidation to produce ATP post-ovulation up until the compacted morula commences glycolysis (Bradley and Swann, 2019). Both processes depend on endogenous lipid stores. Lipoic acid is an important cofactor of several mitochondrial enzymes including pyruvate dehydrogenase (Nowinski et al., 2018). These important roles of lipids in oocytes, likely underlie why otherwise healthy but delipidated oocytes are so efficient at *de novo* lipid synthesis (Aizawa et al., 2019). Together with our observation in the current study that BaP exposure increased mitochondrial superoxide and decreased ΔΨm in mature oocytes (Figure 7), these data support that gestational BaP exposure results in persistent oxidative stress in mature, ovulated oocytes, ultimately reducing developmental competence.

This study reported an in-depth characterization of BaP toxicity on oocytes from the embryonic to postnatal ovary and explored persistent effects of gestational BaP on the F1 ovary and mature F1 oocytes. We confirmed, using novel immunofluorescence microscopy, that *in vitro* BaP exposure induces cytochrome c release in the E13.5 ovary, mediating mitochondrial apoptosis. Further we report that both windows of embryonic ovarian development are equally sensitive to BaP-induced germ cell death and induction of persistent oxidative damage in the ovary. To our knowledge, we are the first to characterize and report on persistent oxidative stress following gestational BaP exposure, resulting in ovarian damage and reduced oocyte developmental competence. In this current study, we were unable to fully characterize the metabolic profile of BaP-exposed oocytes. Future studies should perform a detailed analysis of metabolic endpoints of oocytes exposed to gestational BaP, including oxygen consumption rate of oocytes and embryos.

Cancer Institute of the NIH under award number P30CA062203.

The content is solely the responsibility of the authors and does not necessarily represent the official views of the National Institutes of Health.

AUTHOR CONTRIBUTIONS

DECLARATION OF CONFLICTING INTERESTS

DATA AVAILABILITY

The data underlying this article will be shared on reasonable request to the corresponding author.

REFERENCES

Adhikari, D., Lee, I., Yuen, W. S., and Carroll, J. (2022). Oocyte mitochondria—Key regulators of oocyte function and potential therapeutic targets for improving fertility. *Biol. Reprod.* **106**, 366–377.

Aizawa, R., Ibayashi, M., Tatsumi, T., Yamamoto, A., Kokubo, T., Miyasaka, N., Sato, K., Ikeda, S., Minami, N., and Tsukamoto, S. (2019). Synthesis and maintenance of lipid droplets are essential for mouse preimplantation embryonic development. *Development* **146**, 1–11.

Benador, I. Y., Veliova, M., Liesa, M., and Shirihai, O. S. (2019). Mitochondria bound to lipid droplets: Where ditochondrial dynamics regulate lipid storage and utilization. *Cell Metab.* **29**, 827–835.

Benador, I. Y., Veliova, M., Mahdaviani, K., Petcherski, A., Wikstrom, J. D., Assali, E. A., Acín-Pérez, R., Shum, M., Oliveira, M. F., Cinti, S., *et al.* (2018). Mitochondria bound to lipid droplets have unique bioenergetics, composition, and dynamics that support lipid droplet expansion. *Cell Metab.* **27**, 869–885.

Bianchi, S., Macchiarelli, G., Micara, G., Linari, A., Boninsegna, C., Aragona, C., Rossi, G., Cecconi, S., and Nottola, S. A. (2015). Ultrastructural markers of quality are impaired in human metaphase II aged oocytes: A comparison between reproductive and in vitro aging. *J. Assist. Reprod. Genet.* **32**, 1343–1358.

Biegel, L. B., Flaws, J. A., Hirshfield, A. N., O'Connor, J. C., Elliott, G. S., Ladics, G. S., Silbergeld, E. K., Van Pelt, C. S., Hurtt, M. E., Cook, J. C., *et al.* (1998). 90-day feeding and one-generation reproduction study in Crl: CD BR rats with 17β-estradiol. *Toxicol. Sci.* **44**, 116–142.

Bradley, J., and Swann, K. (2019). Mitochondria and lipid metabolism in mammalian oocytes and early embryos. *Int. J. Dev. Biol.* **63**, 93–103.

Chapin, R. E., Harris, M. W., Davis, B. J., Ward, S. M., Wilson, R. E., Mauney, M. A., Lockhart, A. C., Smialowicz, R. J., Moser, V. C., Burka, L. T., *et al.* (1997). The effects of perinatal/juvenile methoxychlor exposure on adult rat nervous, immune, and reproductive system function. *Fundam. Appl. Toxicol.* **40**, 138–157.

Chiaratti, M. R., Garcia, B. M., Carvalho, K. F., Machado, T. S., da Silva Ribeiro, F. K., and Macabelli, C. H. (2018). The role of mitochondria in the female germline: Implications to fertility and inheritance of mitochondrial diseases. *Cell Biol. Int.* **42**, 711–724.

Collado-Fernandez, E., Picton, H. M., and Dumollard, R. (2012). Metabolism throughout follicle and oocyte development in mammals. *Int. J. Dev. Biol.* **56**, 799–808.

Cooper, R. L., Goldman, J. M., and Vadenbergh, J. G. (1993). Monitoring of the estrous cycle in the laboratory rodent by vaginal lavage. In *Female Reproductive Toxicology* (J. J. Heindel and R. E. Chapin, Eds.), pp. 45–55. Academic Press, Inc., San Diego, CA.

Coticchio, G., Sereni, E., Serrao, L., Mazzone, S., Iadarola, I., and Borini, A. (2004). What criteria for the definition of oocyte quality? *Ann. N.Y. Acad. Sci.* **1034**, 132–144.

Dalleau, S., Baradat, M., Guéraud, F., and Huc, L. (2013). Cell death and diseases related to oxidative stress: 4-hydroxynonenal (HNE) in the balance. *Cell Death Differ.* **20**, 1615–1630.

de Sousa Lopes, S. M. C., Hayashi, K., and Surani, M. A. (2007). Proximal visceral endoderm and extraembryonic ectoderm regulate the formation of primordial germ cell precursors. *BMC Dev. Biol.* **7**, 140.

Devine, P. J., Perreault, S. D., and Luderer, U. (2012). Roles of reactive oxygen species and antioxidants in ovarian toxicity. *Biol. Reprod.* **86**, 1–10.

Dunning, K. R., Cashman, K., Russell, D. L., Thompson, J. G., Norman, R. J., and Robker, R. L. (2010). Beta-oxidation is essential for mouse oocyte developmental competence and early embryo development. *Biol. Reprod.* **83**, 909–918.

Dunning, K. R., Russell, D. L., and Robker, R. L. (2014). Lipids and oocyte developmental competence: The role of fatty acids and β-oxidation. *Reproduction* **148**, R15–R27.

Eling, T. E., Thompson, D. C., Foureman, G. L., Curtis, J. F., and Hughes, M. F. (1990). Prostaglandin H synthase and xenobiotic oxidation. *Annu. Rev. Pharmacol. Toxicol.* **30**, 1–45.

Eskes, R., Antonsson, B., Osen-Sand, A., Montessuit, S., Richter, C., Sadoul, R., Mazzei, G., Nichols, A., and Martinou, J. C. (1998). Bax-induced cytochrome C release from mitochondria is independent of the permeability transition pore but highly dependent on Mg2+ ions. *J. Cell Biol.* **143**, 217–224.

Feng, R., Han, J., Ziegler, J., Yang, M., and Castranova, V. (2012). Apaf-1 deficiency confers resistance to ultraviolet-induced apoptosis in mouse embryonic fibroblasts by disrupting reactive oxygen species amplification production and mitochondrial pathway. *Free Radic. Biol. Med.* **52**, 889–897.

Ferraro, E., Corvaro, M., and Cecconi, F. (2003). Physiological and pathological roles of Apaf1 and the apoptosome. *J. Cell. Mol. Med.* **7**, 21–34.

Findlay, J. K., Hutt, K. J., Hickey, M., and Anderson, R. A. (2015). How is the number of primordial follicles in the ovarian reserve established? *Biol. Reprod.* **93**, 1–7.

Forman, H. J., Zhang, H., and Rinna, A. (2009). Glutathione: Overview of its protective roles, measurement, and biosynthesis. *Mol. Aspects Med.* **30**, 1–12.

Guérin, P., El Mouatassim, S., and Ménézo, Y. (2001). Oxidative stress and protection against reactive oxygen species in the pre-implantation embryo and its surroundings. *Hum. Reprod. Update* **7**, 175–189.

Gulyas, B. J., and Mattison, D. R. (1979). Degeneration of mouse oocytes in response to polycyclic aromatic hydrocarbons. *Anat. Rec.* **193**, 863–881.

Han, J., Flemington, C., Houghton, A. B., Gu, Z., Zambetti, G. P., Lutz, R. J., Zhu, L., and Chittenden, T. (2001). Expression of bbc3, a pro-apoptotic BH3-only gene, is regulated by diverse cell death and survival signals. *Proc. Natl. Acad. Sci. U.S.A* **98**, 11318–11323.

Hu, T., Pan, Z., Yu, Q., Mo, X., Song, N., Yan, M., Zouboulis, C. C., Xia, L., and Ju, Q. (2016a). Benzo(a)pyrene induces interleukin (IL)-6 production and reduces lipid synthesis in human SZ95 sebocytes via the aryl hydrocarbon receptor signaling pathway. *Environ. Toxicol. Pharmacol.* **43**, 54–60.

Hu, T., Wang, D., Yu, Q., Li, L., Mo, X., Pan, Z., Zouboulis, C. C., Peng, L., Xia, L., and Ju, Q. (2016b). Aryl hydrocarbon receptor negatively regulates lipid synthesis and involves in cell differentiation of SZ95 sebocytes in vitro. *Chem. Biol. Interact.* **258**, 52–58.

Jarc, E., and Petan, T. (2019). Lipid droplets and the management of cellular stress. *Yale J. Biol. Med.* **92**, 435–452.

Jules, G. E., Pratap, S., Ramesh, A., and Hood, D. B. (2012). In utero exposure to benzo(a)pyrene predisposes offspring to cardiovascular dysfunction in later-life. *Toxicology* **295**, 56–67.

Kasianowicz, J., Benz, R., and McLaughlin, S. (1984). The kinetic mechanism by which CCCP (carbonyl cyanide m-chlorophenylhydrazone) transports protons across membranes. *J. Membr. Biol.* **82**, 179–190.

Kerr, J. B., Hutt, K. J., Michalak, E. M., Cook, M., Vandenberg, C. J., Liew, S. H., Bouillet, P., Mills, A., Scott, C. L., Findlay, J. K., *et al.* (2012). DNA damage-induced primordial follicle oocyte apoptosis and loss of fertility require TAp63-mediated induction of Puma and Noxa. *Mol. Cell* **48**, 343–352.

Kinner, A., Wu, W., Staudt, C., and Iliakis, G. (2008). Gamma-H2AX in recognition and signaling of DNA double-strand breaks in the context of chromatin. *Nucleic Acids Res.* **36**, 5678–5694.

Koubova, J., Menke, D. B., Zhou, Q., Capel, B., Griswold, M. D., and Page, D. C. (2006). Retinoic acid regulates sex-specific timing of meiotic initiation in mice. *Proc. Natl. Acad. Sci. U.S.A.* **103**, 2474–2479.

Kushnir, V. A., Ludaway, T., Russ, R. B., Fields, E. J., Koczor, C., and Lewis, W. (2012). Reproductive aging is associated with decreased mitochondrial abundance and altered structure in murine oocytes. *J. Assist. Reprod. Genet.* **29**, 637–642.

Láscarez-Lagunas, L., Martinez-Garcia, M., and Colaiácovo, M. (2020). SnapShot: Meiosis—Prophase I. *Cell* **181**, 1442–1442.

Li, F., Xiang, B., Jin, Y., Li, C., Ren, S., Wu, Y., Li, J., and Luo, Q. (2020). Hepatotoxic effects of inhalation exposure to polycyclic aromatic hydrocarbons on lipid metabolism of C57BL/6 mice. *Environ. Int.* **134**, 1–8.

Li, W. D., Yu, S., Luo, S. M., Shen, W., Yin, S., and Sun, Q. Y. (2019). Melatonin defends mouse oocyte quality from benzo[ghi]perylene-induced deterioration. *J. Cell. Physiol.* **234**, 6220–6229.

Lim, J., Kong, W., Lu, M., and Luderer, U. (2016). The mouse fetal ovary has greater sensitivity than the fetal testis to benzo[a]pyrene-induced germ cell death. *Toxicol. Sci.* **152**, 372–381.

Lim, J., Lawson, G. W., Nakamura, B. N., Ortiz, L., Hur, J. A., Kavanagh, T. J., and Luderer, U. (2013). Glutathione-deficient mice have increased sensitivity to transplacental benzo[a]pyrene-induced premature ovarian failure and ovarian tumorigenesis. *Cancer Res.* **73**, 908–917.

Lim, J., and Luderer, U. (2018). Glutathione deficiency sensitizes cultured embryonic mouse ovaries to benzo[a]pyrene-induced germ cell apoptosis. *Toxicol. Appl. Pharmacol.* **352**, 38–45.

Lim, J., Nakamura, B. N., Mohar, I., Kavanagh, T. J., and Luderer, U. (2015). Glutamate cysteine ligase modifier subunit (Gclm) null mice have increased ovarian oxidative stress and accelerated age-related ovarian failure. *Endocrinology* **156**, 3329–3343.

Lim, J., Ramesh, A., Shioda, T., Parada, K. L., and Luderer, U. (2022). Sex differences in embryonic gonad transcriptomes and benzo[a]pyrene metabolite levels after transplacental exposure. *Endocrinology* **163**, 1–17.

Liu, L., Trimarchi, J. R., Navarro, P., Blasco, M. A., and Keefe, D. L. (2003). Oxidative stress contributes to arsenic-induced telomere attrition, chromosome instability, and apoptosis. *J. Biol. Chem.* **278**, 31998–32004.

Luderer, U., Lim, J., Ortiz, L., Nguyen, J. D., Shin, J. H., Allen, B. D., Liao, L. S., Malott, K., Perraud, V., Wingen, L. M., *et al.* (2022). Exposure to environmentally relevant concentrations of ambient fine particulate matter (PM2.5) depletes the ovarian follicle reserve and causes sex-dependent cardiovascular changes in apolipoprotein E null mice. *Part. Fibre Toxicol.* **19**, 5–21.

Luderer, U., Myers, M. B., Banda, M., McKim, K. L., Ortiz, L., and Parsons, B. L. (2017). Ovarian effects of prenatal exposure to benzo[a]pyrene: Roles of embryonic and maternal glutathione status. *Reprod. Toxicol.* **69**, 187–195.

Malott, K. F., Reshel, S., Ortiz, L., and Luderer, U. (2022). Glutathione deficiency decreases lipid droplet stores and increases reactive oxygen species in mouse oocytes. *Biol. Reprod.* **106**, 1218–1231.

Matikainen, T. M., Moriyama, T., Morita, Y., Perez, G. I., Korsmeyer, S. J., Sherr, D. H., and Tilly, J. L. (2002). Ligand activation of the aromatic hydrocarbon receptor transcription factor drives Bax-dependent apoptosis in developing fetal ovarian germ cells. *Endocrinology* **143**, 615–620.

Mattison, D. R. (1980). Morphology of oocyte and follicle destruction by polycyclic aromatic hydrocarbons in mice. *Toxicol. Appl. Pharmacol.* **53**, 249–259.

Mattison, D. R., and Thorgeirsson, S. S. (1979). Ovarian aryl hydrocarbon hydroxylase activity and primordial oocyte toxicity of polycyclic aromatic hydrocarbons in mice. *Cancer Res.* **39**, 3471–3475.

Mishra, B., Ortiz, L., and Luderer, U. (2016). Charged iron particles, components of space radiation, destroy ovarian follicles. *Hum. Reprod.* **31**, 1816–1826.

Mishra, B., Ripperdan, R., Ortiz, L., and Luderer, U. (2017). Very low doses of heavy oxygen ion radiation induce premature ovarian failure. *Reproduction* **154**, 123–133.

Motta, P. M., Nottola, S. A., Makabe, S., Heyn, R., and Jansen, R. (2000). Mitochondrial morphology in human fetal and adult female germ cells. *Hum. Reprod.* **15**, 129–147.

Myers, M., Britt, K. L., Wreford, N. G. M., Ebling, F. J. P., and Kerr, J. B. (2004). Methods for quantifying follicular numbers within the mouse ovary. *Reproduction* **127**, 569–580.

Myers, M., Morgan, F. H., Liew, S. H., Zerafa, N., Gamage, T. U., Sarraj, M., Cook, M., Kapic, I., Sutherland, A., Scott, C. L., *et al.* (2014). PUMA regulates germ cell loss and primordial follicle endowment in mice. *Reproduction* **148**, 211–219.

Nakano, K., and Vousden, K. H. (2001). PUMA, a novel proapoptotic gene, is induced by p53. *Mol. Cell.* **7**, 683–694.

Neuschäfer-rube, F., Schraplau, A., Schewe, B., Lieske, S., Krützfeldt, J., Ringel, S., Henkel, J., Birkenfeld, A. L., and Püschel, G. P. (2015). Arylhydrocarbon receptor-dependent m Indy (Slc13a5) induction as possible contributor to benzo[a]pyrene-induced lipid accumulation in hepatocytes. *Toxicology* **337**, 1–9.

Nowinski, S. M., Van Vranken, J. G., Dove, K. K., and Rutter, J. (2018). Impact of mitochondrial fatty acid synthesis on mitochondrial biogenesis. *Curr. Biol.* **28**, R1212–R1219.

NRC. (2011). *Guide for the Care and Use of Laboratory Animals*, 8th ed. National Research Council, National Academy of Sciences, Washington, DC.

Orrenius, S., Gogvadze, V., and Zhivotovsky, B. (2007). Mitochondrial oxidative stress: Implications for cell death. *Annu. Rev. Pharmacol. Toxicol.* **47**, 143–183.

Paczkowski, M., Schoolcraft, W. B., and Krisher, R. L. (2014). Fatty acid metabolism during maturation affects glucose uptake and is essential to oocyte competence. *Reproduction* **148**, 429–439.

Penning, T. M., Ohnishi, S. T., Ohnishi, T., and Harvey, R. G. (1996). Generation of reactive oxygen species during the enzymatic oxidation of polycyclic aromatic hydrocarbon trans-dihydrodiols catalyzed by dihydrodiol dehydrogenase. *Chem Res Toxicol.* **9**, 84–92.

Pepling, M. E. (2012). Follicular assembly: Mechanisms of action. *Reproduction* **143**, 139–149.

Pepling, M. E., and Spradling, A. C. (2001). Mouse ovarian germ cell cysts undergo programmed breakdown to form primordial follicles. *Dev. Biol.* **234**, 339–351.

Pepling, M. E., Wilhelm, J. E., O'Hara, A. L., Gephardt, G. W., and Spradling, A. C. (2007). Mouse oocytes within germ cell cysts and primordial follicles contain a Balbiani body. *Proc. Natl. Acad. Sci. U.S.A.* **104**, 187–192.

Plíšková, M., Vondrácek, J., Vojtesek, B., Kozubík, A., and Machala, M. (2005). Deregulation of cell proliferation by polycyclic aromatic hydrocarbons in human breast carcinoma MCF-7 cells reflects both genotoxic and nongenotoxic events. *Toxicol. Sci.* **83**, 246–256.

Prates, E. G., Nunes, J. T., and Pereira, R. M. (2014). A role of lipid metabolism during cumulus-oocyte complex maturation: Impact of lipid modulators to improve embryo production. *Mediators Inflamm.* **2014**, 692067–692011.

Ramalho-Santos, J., and Amaral, S. (2013). Mitochondria and mammalian reproduction. *Mol. Cell. Endocrinol.* **379**, 74–84.

Ramalho-Santos, J., Varum, S., Amaral, S., Mota, P. C., Sousa, A. P., and Amaral, A. (2009). Mitochondrial functionality in reproduction: From gonads and gametes to embryos and embryonic stem cells. *Hum. Reprod. Update.* **15**, 553–572.

Ramesh, A., Inyang, F., Hood, D. B., Archibong, A. E., Knuckles, M. E., and Nyanda, A. M. (2001). Metabolism, bioavailability, and toxicokinetics of benzo(alpha)pyrene in F-344 rats following oral administration. *Exp. Toxicol. Pathol.* **53**, 275–290.

Safranski, T., Lamberso, W. R., and Keisler, D. H. (1993). Correlations among three measures of puberty in mice and relationships with estradiol concentration and ovulation. *Biol. Reprod.* **48**, 669–673.

Sobinoff, A. P., Pye, V., Nixon, B., Roman, S. D., and McLaughlin, E. A. (2012). Jumping the gun: Smoking constituent BaP causes premature primordial follicle activation and impairs oocyte fusibility through oxidative stress. *Toxicol. Appl. Pharmacol.* **260**, 70–80.

Stringer, J. M., Winship, A., Zerafa, N., Wakefield, M., and Hutt, K. (2020). Oocytes can efficiently repair DNA double-strand breaks to restore genetic integrity and protect offspring health. *Proc. Natl. Acad. Sci. U.S.A.* **117**, 11513–11522.

Sui, L., Nie, J., Xiao, P., Yan, K., Zhang, H., Liu, J., Zhang, H., Cui, K., Lu, K., and Liang, X. (2020). Maternal benzo[a]pyrene exposure is correlated with the meiotic arrest and quality deterioration of offspring oocytes in mice. *Reprod. Toxicol.* **93**, 10–18.

Valsangkar, D., and Downs, S. M. (2013). A requirement for fatty acid oxidation in the hormone-induced meiotic maturation of mouse oocytes. *Biol. Reprod.* **89**, 1–9.

van Lipzig, M. M. H., Vermeulen, N. P. E., Gusinu, R., Legler, J., Frank, H., Seidel, A., and Meerman, J. H. N. (2005). Formation of estrogenic metabolites of benzo[a]pyrene and chrysene by cytochrome P450 activity and their combined and supra-maximal estrogenic activity. *Environ. Toxicol. Pharmacol.* **19**, 41–55.

Walther, T. C., and Farese, R. V. (2009). The life of lipid droplets. *Biochim. Biophys. Acta* **1791**, 459–466.

Walther, T. C., and Farese, R. V. (2012). Lipid droplets and cellular lipid metabolism. *Annu. Rev. Biochem.* **81**, 687–714.

Wear, H. M., McPike, M. J., and Watanabe, K. H. (2016). From primordial germ cells to primordial follicles: A review and visual representation of early ovarian development in mice. *J. Ovarian Res.* **9**, 11.

Wu, J., Ramesh, A., Nayyar, T., and Hood, D. B. (2003). Assessment of metabolites and AhR and CYP1A1 mRNA expression subsequent to prenatal exposure to inhaled benzo(a)pyrene. *Int. J. Dev. Neurosci.* **21**, 333–346.

Xue, W., and Warshawsky, D. (2005). Metabolic activation of polycyclic and heterocyclic aromatic hydrocarbons and DNA damage: A review. *Toxicol. Appl. Pharmacol.* **206**, 73–93.

Zhang, M., Miao, Y., Chen, Q., Cai, M., Dong, W., Dai, X., Lu, Y., Zhou, C., Cui, Z., and Xiong, B. (2018). BaP exposure causes oocyte meiotic arrest and fertilization failure to weaken female fertility. *FASEB J.* **32**, 342–352.

Zhang, X., Wang, T., Song, J., Deng, J., and Sun, Z. (2020). Study on follicular fluid metabolomics components at different ages based on lipid metabolism. *Reprod. Biol. Endocrinol.* **18**, 1–8.

Zhong, H., and Yin, H. (2015). Role of lipid peroxidation derived 4-hydroxynonenal (4-HNE) in cancer: Focusing on mitochondria. *Redox Biol.* **4**, 193–199.